Astron. Astrophys. 353, 666–690 (2000)

ASTRONOMY AND ASTROPHYSICS

The infrared triplet lines of ionized calcium as a diagnostic tool for F, G, K-type stellar atmospheres

Yves Chmielewski

Observatoire de Genève, 1290 Sauverny, Switzerland (Yves.Chmielewski@obs.unige.ch)

Received 26 March 1999 / Accepted 10 November 1999

Abstract. LTE calculations of the profiles of the infrared triplet lines of ionized calcium in the spectrum of F, G and K stars are described in detail with explicit quantitative consideration of their perturbation by hydrogen Paschen lines. The results of such calculations obtained with five different solar model atmospheres are discussed. The sensitivity of the profiles to changes in basic stellar atmospheric parameters is illustrated. The flux in the center of the $\lambda 8542$ Å line is related empirically to the Mount-Wilson chromospheric activity indicator R'_{HK}. The predictive power of observations of the infrared triplet lines is then summed up.

Key words: line: profiles – radiative transfer – stars: fundamental parameters – stars: late-type

1. Introduction

Calcium is one of the best represented and best studied elements in the visible spectrum of the cool F, G and K stars. Lines of calcium cover a wide variety of excitation conditions and line strengths, and especially accurate atomic parameters are available. The dramatic improvement brought about by modern silicon array detectors has led investigators to focus more on the red and near infrared part of the spectrum. The infrared triplet lines of ionized calcium (Ca II IRT) at 8498, 8542 and 8662 Å are quite prominent features in this region of the spectrum of late type stars. On the one hand, the profiles of the extended wings of these very strong lines have been shown to be a good signature of the temperature distribution in the atmosphere of the stars. On the other hand, their central intensity is quite sensitive to the degree of activity of their outer layers. G. Cayrel de Strobel and her collaborators (to which I am priviliged to belong) systematically made use of the latter property, albeit in a purely qualitative way. In view of this, they usually record high quality spectra of the relevant spectral region for each star under investigation. Over recent years, G. Smith, J.J. Drake and collaborators showed that the Ca II IRT could be used for a more quantitative discussion of stellar atmospheric properties. A more quantitative use of our good quality observations thus seems advisable. Therefore, I re-examined the solar case as a reference for further quantitative high resolution spectroscopic stellar studies. The data relevant to the study of the Ca II IRT being quite scattered in the literature, it appeared useful to write this paper as a *vade mecum* for those wishing to use these lines as an element of diagnosis of the cool stellar atmospheres. The relevant literature is reviewed in some detail in Sect. 2. Contamination by telluric lines and continuum location problems are discussed in Sect. 3. In Sect. 4 synthetic profiles of the Ca II IRT lines in the solar flux spectrum are presented for a set of two empirical solar model atmospheres and three theoretical constant-flux model solar photospheres. The perturbation by neighbouring hydrogen Paschen lines is discussed for the first time in quantitative terms. Figures illustrating the response of the line profiles to changes in the basic stellar photospheric parameters can be found in Sect. 5. Finally, in Sect. 6, existing scattered data of diffferent sources on the central depths of the Ca II IRT lines is gathered and an improved relationship is established between this data and other quantitative chromospheric activity indicators obtained from observations of the emission reversals in the Ca II resonance H and K lines.

2. Review of previous investigations

2.1. Neutral calcium, Ca I

The first fully detailed study of all useful calcium lines in the solar spectrum was published by Holweger (1972) who gave a complete evaluation of the relevant atomic data available at that time. The solar abundance of calcium resulting from his investigation is $\log \epsilon_{\odot}(Ca) = \log(N(Ca)/N(H)) + 12 = 6.36 \pm 0.07$.

Later, at Oxford, G. Smith and his collaborators determined accurate laboratory oscillator strengths and damping parameters for collisions with helium around $2000\,K$ for many useful lines of neutral calcium (Smith & O'Neill, 1975; O'Neill & Smith, 1980; Smith & Raggett, 1981; Smith, 1988). The helium damping parameters were semi-empirically extended to collisions with neutral hydrogen at solar temperatures (see O'Neill & Smith 1980 for details). These data were then used to perform absolute analyses of the Ca I lines in a small number of stars. In an iterative procedure these investigators evaluated the excitation and ionisation equilibrium from a set of weak Fe I and Fe II lines, derived a value of the microturbulence from medium strong Ca I lines and found the value of the surface gravity

from the damping wings of the strong Ca I line at 6162 Å. For the solar case, Smith (1981) obtained an abundance of calcium $\log \epsilon_{\odot}(Ca) = 6.36 \pm 0.02$ with the empirical solar model atmosphere of Holweger & Müller (1974), in complete agreement with the value already derived by Holweger (1972).

2.2. Statistical equilibrium in Ca I

In the case of the atmospheres of the Sun and Procyon, Watanabe & Steenbock (1985) investigated the statistical equilibrium of the level populations of a Ca model atom consisting in 16 levels of Ca I, 3 levels of Ca II (to allow for the ionization of the doubly excited levels of Ca I), plus the ground state of Ca III. They found no deviations from Local Thermodynamic Equilibrium (LTE) populations in the Ca II levels (the dominant ion in later type stellar atmospheres), and they mapped the abundance errors resulting from departures from LTE in the different lines of Ca I. They concluded that the global non-LTE effects on the determination of the calcium abundance are quite small in the case of the Sun, but are noticeable in the atmosphere of Procyon, although remaining small for weak lines ($W_{\lambda} < 80$ mÅ).

Drake (1991), using new computational techniques, extended the work of Watanabe & Steenbock by looking at the behaviour of the formation of lines in the same model Ca atom under a much wider set of model atmospheric conditions. He considered sets of model atmospheres typical of: (1) solar type dwarfs with varying temperatures, (2) cool giants with varying gravities and (3) solar temperature metal-deficient dwarfs with varying metallicities. His results confirm the conclusions of Watanabe & Steenbock for the solar case. No significant non-LTE effect in the level populations of Ca II is found for any of the model atmospheres considered. Departures from LTE in Ca I are dominated by a general overionization showing an unexpectedly complicated behaviour with the basic stellar atmospheric parameters, often explained by the behaviour of the continuous absorption coefficient in the ultraviolet. The paper provides non-LTE abundance correction factors for the lines of each individual multiplet of Ca I for the different model atmospheres and one of its general conclusions is that "non-LTE effects in Ca I in solar type dwarf stars are likely to be insignificant, but these effects become increasingly significant toward lower gravity stars".

2.3. The ionized calcium infrared triplet lines

The H and K resonance lines of ionized calcium, Ca II, are the most characteristic features of the spectra of late type stars and they are widely used for the study of their chromospheric activity. The infrared triplet lines of Ca II (Ca II IRT) are also quite conspicuous features of the spectra of these stars. Since the advent of solid state detectors they are readily observed with high resolution, high signal-to-noise ratio and good photometric accuracy. The extended wings of these dark lines probe a wide range of photospheric layers, and are thus sensitive to the run of the temperature distribution with depth. Their cores are so opaque that they are formed in the uppermost atmospheric layers (chromospheres) and their central depths have also been shown to provide good indicators of chromospheric activity (see e.g., Linsky et al. 1979, Cayrel et al. 1983, Foing et al. 1989).

Further interest in the Ca II IRT arose when Jones et al. (1984) claimed on empirical grounds that the strength of these lines provided a very good luminosity indicator in the context of the evaluation of giant-to-dwarf ratios in stellar systems population synthesis; they advocated the existence of a single-valued relation between their strength and stellar surface gravity. This observation was further discussed and clarified by Diaz et al. (1989) who found instead a biparametric behaviour of the Ca II triplet with gravity and metallicity. Their findings were that, at high metallicities, gravity is the dominant parameter, whereas, at low metallicities, metal abundance is the leading parameter. For stars of spectral type later than K3, Zhou (1991) found some dependance of the IRT absorption on temperature; yet, as long as the metallicity differences are not too large, the IRT intensities allow a clear separation of giant from dwarf stars. Ginestet et al. (1994) set up a spectral classification scheme in the near infrared ($\lambda\lambda$ 8380–8780 Å) where the Ca II 8542 Å line plays a key role for the classification of stars of types G to M. Carquillat et al. (1997) published a useful atlas of spectra of stars of types F6 to M in the 8400–8800 Å region, at 2 Å resolution, illustrating the spectral changes with spectral type and luminosity class. The empirical approach is reconsidered in detail and summarized by Mallik (1997) who also provides an interesting atlas of spectra of the three IRT lines observed at a rather high resolution (0.4 Å) for stars of spectral types from F7 to M4 of all luminosity classes and a large range of metallicities.

On the theoretical side, the findings of Jones et al. (1984) led G. Smith, J.J. Drake and co-workers in particular to include the Ca II IRT lines as key features in the line list for their studies of the spectrum of calcium in late F to early K type stars. On the basis of LTE spectrum synthesis calculations Smith & Drake (1987) investigated the sensivity of the wings of the strongest line of the Ca II IRT at 8542 Å to the basic stellar atmospheric parameters for dwarf and subgiant solar-type stars. They found in fact little sensitivity to the surface gravity, a much larger effect from metallicity increasing with temperature, and a sensitivity to effective temperature which starts becoming significant only at the higher end of the temperature interval considered $(5100 \leq T_{\rm eff} \leq 6400\,K)$. They were also able to obtain good fits to the observed wings of this line in spectra of the stars $\tau\ Cet$ and $\eta\ Cas\ A$. Smith & Drake (1988) obtained excellent, very detailed fits to the solar intensity profiles of the wings of the three Ca II IRT lines at two μ-positions on the solar disk from LTE synthetic profiles calculated using the solar empirical model photosphere of Holweger & Müller (1974). Adopting the reliable oscillator strengths given by Gallagher (1967) and the calcium abundance from Smith (1981), they derive accurate hydrogen broadening parameters for the three lines.

Smith & Drake (1990) again investigated the sensitivity of the Ca II 8542 Å line, but this time for a range of atmospheric parameters representative of cool giant stars. Again, the sensitivity of the computed profile to metallicity is the largest. Although larger for the lower values of $\log g$ than in the case of dwarfs, the sensitivity to surface gravity is still weak. As for the effects

of changes in effective temperature they remain quite small. Erdelyi-Mendes & Barbuy (1991) calculated synthetic spectra of the Ca II IRT region for stars of cooler effective temperature ($4000 \leq T_{\rm eff} \leq 5480\,K$), but with a "low resolution" approach devised for direct comparison with the empirical data of Diaz et al. (1989), where they take into account the effect of numerous atomic and molecular lines in the spectral region. They show in particular the importance of the contribution to total absorption of CN and TiO bands at the lower temperatures. Their Fig. 1 illustrates the impossibility of locating the real continuum in M stars. They investigate the sensitivity of global absorption in the region of the Ca II IRT lines to the basic stellar atmospheric parameters, confirming, with restrictions, the empirical conclusions of Diaz et al.

These studies have described the response of the Ca II IRT lines to changes in the basic photospheric parameters within a given grid of model stellar photospheres. However the theory tells us that the detailed shape of the extended wings of very strong lines, such as the Ca II IRT, reflects the variation of the source function with the depth in the atmosphere. When the conditions of LTE apply, this is a direct function of the distribution of temperature with depth. The observed shape of very dark lines should thus allow us to check the validity of the temperature distribution adopted for the analysis of the spectrum of a given star. In the special case of the Ca II line at 8542 Å, this property was applied by Drake & Smith (1991) to build an empirical model atmosphere for their very detailed study of the spectra of calcium and iron in the K0 giant Pollux. It has also been used to assess that scaled solar empirical Holweger-Müller temperature distributions were adequate for the study of the chromospherically active dwarfs $\epsilon\ Eri$ (Drake & Smith 1993) and $\xi\ Boo\ A$ (Ruck & Smith 1995), whereas a theoretical flux-constant MARCS model atmosphere (i.e. computed according to Gustafsson et al. 1975) was more appropriate for the analysis of the spectrum of the subdwarf Groombridge 1830 (Smith et al. 1992). From high resolution spectra of Ca II $\lambda 8542$ in four dwarfs and two giants in the Hyades cluster, Smith & Ruck (1997) derived the metallicity of the dwarfs and the gravity of the giants (the metallicity of the latter being determined, independently of gravity, by the Mg I $\lambda 8806$ line).

2.4. Departures from LTE in the Ca II IRT

Within the entire range of spectral types under consideration (late F, G and early K dwarfs and giants), Ca II turns out to be the dominant ionization stage. The investigations of the statiscal equilibrium in Ca I by Watanabe & Steenbock (1985) and Drake (1991) have already suggested that the global population of Ca II is never significantly altered by departures from LTE. Jørgensen et al. (1992) looked more specifically at the effects of departures from LTE on the Ca II IRT lines for a complete set of MARCS model photospheres. For that purpose they used a model calcium atom comprising 8 levels in Ca I, 5 levels in Ca II, plus the ground state of Ca III. Unfortunately, there is no discussion of the effects on the detailed profile of these lines: they discuss only the effects on the combined integrated equivalent widths. Nor do they examine the effect of an eventual chromospheric temperature rise, known to affect the central core intensities, considering that such an effect will not alter significantly the global equivalent width. However, they conclude that, if the line cores are indeed out of LTE, the Ca II IRT line wings are formed in conditions close to LTE, and the effect of departures from LTE on the equivalent widths is always negligible. The largest non-LTE effects are found at high temperatures and gravities. They also point out that the dependence of the equivalent width on gravity is higher at the higher metallicities and that, at low metallicities, the dependence on $T_{\rm eff}$ is greater than that on $\log g$. The interesting point they make is that the complicated behaviour of the equivalent widths with the variations of the stellar atmospheric parameters is largely dependent on whether the natural or the collisional broadening mechanism is dominant in the atmosphere considered. It is worth mentioning that these authors adopted a value for the collision broadening parameters that differs from the value derived by Smith & Drake (1988) by 25% or so; this may affect the behaviour of the calculated line strengths.

3. Observations and reduction problems

The first step in an investigation of the Ca II IRT lines in stellar spectra is to consider the solar reference case. This is the case for which the best observations are available and the physics of which is best known. Many stellar spectroscopic analyses are carried out differentially with respect to a solar spectrum recorded under the same observational conditions as the program stellar spectrum. In this first part devoted to the solar case, the computed synthetic profiles are compared with both the best quality solar flux spectrum available (the Solar Flux Atlas of Kurucz et al. 1984) and a reflected sunlight spectrum recorded under "stellar" conditions with a typical high resolution stellar spectrograph. G. Cayrel de Strobel has accumulated a large number of reference solar (moonlight) spectra of the region of the first two Ca II IRT lines, which she kindly allowed me to use. Among these, some were recorded with the coudé spectrograph of the Canada-France-Hawaii (CFH) telescope atop Maunea Kea, Hawaii, a very dry site at 4200m altitude, and are almost devoid of water vapour absorption. One of them, recorded in 1983, was selected as the reference spectrum for this study.

Many of the investigations of the Ca II IRT in stellar spectra have ignored the third line at 8662.14 Å, probably for convenience because the two other lines at 8498.02 and 8542.09 Å fit on a single frame in modern high-resolution spectrographs. Moreover, as shown by Smith & Drake (1988) for the solar spectrum, this third line is the only one for which a measurable asymmetry gives some evidence of a small but significant perturbation by one of the hydrogen Paschen lines (here, P13) which fall in the red wings of the three Ca II lines. Often, stellar investigations concentrate exclusively on the strongest of the three Ca II IRT lines at $\lambda 8542$ which is the least blended and conveys all the information which can be extracted from the triplet.

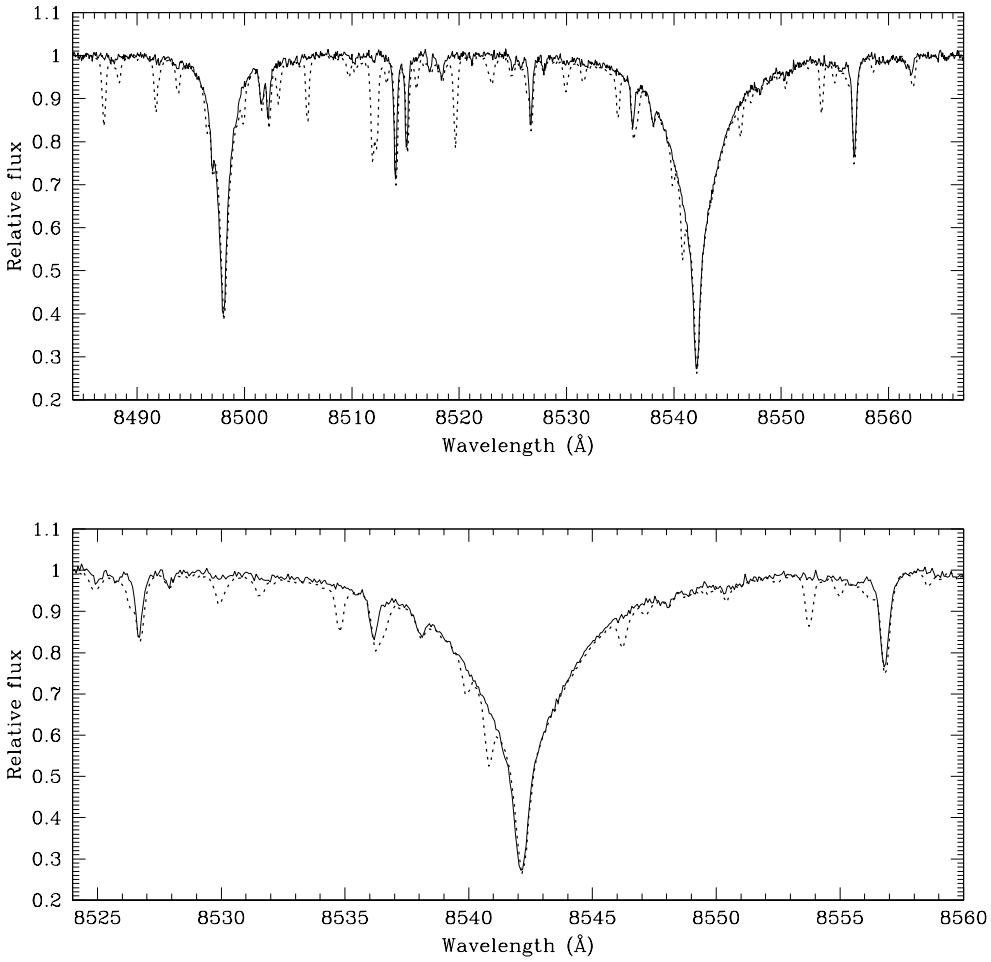

Fig. 1. Telluric water vapour lines in the region of the Ca II IRT lines. Top: the solid line shows a spectrum recorded under very dry conditions and the dotted line shows a spectrum recorded under conditions of exceptionally high water absorption. Bottom: same data enlarged for the $\lambda 8542$ line region.

3.1. Water vapour contamination

Contrary to what is claimed in a number of papers, the whole wavelength region is in fact appreciably polluted by telluric water vapour absorption. In Fig. 1, the selected CFH solar spectrum (solid line) is compared with a spectrum recorded also by G. Cayrel de Strobel but with the Aurélie coudé spectrograph of the Observatoire de Haute Provence (OHP) 1.52m telescope in 1990 (dotted line) during a period of exceptionally high water vapour absorption. The bottom box of Fig. 1 is just a close-up of the same data centered on the most important Ca II $\lambda 8542$ line. These figures illustrate how important it is to try and minimize the water vapour contamination and show which regions of the continuum and line profiles stay unperturbed.

3.2. Definition of the continuum location

An accurate definition of the location of the local continuum is essential if we want to carry out precise fits of the observations by synthetic calculations. On their highest quality and resolution solar intensity spectra of the 8450–8702 Å region obtained with the Fourier Transform Spectrometer at the Mac Math Solar Telescope (Kitt Peak), Smith & Drake (1988) identify ten continuum points where the depression is less than 0.5%, with a huge gap of 105 Å (8473.0–8577.5 Å) where no real continuum point is found. In the same way as for the intensity data, on the Solar Flux Atlas the continuum has been carefully set from the consideration of very long wavelength scans. This cannot equally carefully be done on typical stellar spectrograms. Depending on the resolution mode, a single frame recorded with a typical stellar high resolution spectrograph in current use covers a spectral region of width varying between 75 and 200 Å. Even after applying the usual "flat-fielding" techniques, the spectrograms are generally far from being flat and a reasonable approximation of the continuum requires at least a third order polynomial or sliding polynomials or splines defined by at least 5 to 6 reference points. This implies average distances between reference points of 15 to 30 Å. This lack of real continuum window in the vicinity of the first two Ca II IRT lines is further illustrated by the solar synthetic spectra in Fig. 2. The situation gets more and more difficult as one goes towards cooler stars. Fig. 1 of Zhou (1991) shows how hazardous the continuum normalization can become for stars of the late-K and M types.

On these short "stellar" wavelength scans, it seems indeed almost impossible to accurately define the run of the continuum without recourse to some kind of theoretical prediction. Therefore, as in usual reduction procedures, I first identified windows of higher local intensity, but then normalized the observed spectrum by assigning to them the residual depths pre-

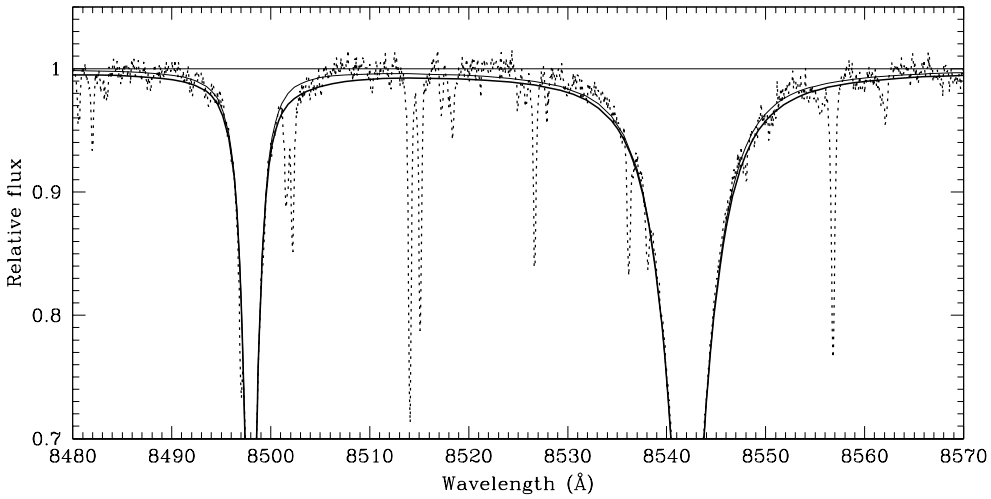

Fig. 2. Continuum location. Dotted line: observed CFH spectrum normalized "classically" through local higher intensity points. Thin solid line: synthetic spectrum with only the Ca II IRT lines. Thick solid line: same synthetic spectrum, but taking into account the absorption by hydrogen Paschen lines.

dicted by a "best fit" synthetic spectrum. Formally, the predicted synthetic depths depend on the model atmosphere and line data used in calculating the synthetic spectrum; the continuum normalization is thus an iterative process. The sensitivity of the local pseudo-continuum points to the choice of the model atmosphere turns out to be weak, so that the normalization process converges very quickly and needs not be repeated for relatively small changes of the parameters of the synthetic spectrum calculation. We shall see in Sect. 5 that explicitly taking into account the absorption by the hydrogen Paschen lines in the region results mainly, in the solar case, in appreciably lowering the apparent continuum level (Fig. 2). Thus, for consistency, when it is deemed necessary to take into account the contribution of Paschen lines, this must be done also for the continuum normalization of stellar observations. Experience shows that the constraints introduced by the fit to the calculated pseudo-continuum windows does not lower the diagnosis capabilities of the Ca II IRT profile fitting.

For stars of the late-K and M types, detailed synthetic calculations of the contribution of the molecular bands, such as those reported by Erdelyi-Mendez & Barbuy (1991), should be necessary.

4. The solar case

The absorption coefficient in the extended wings of very strong lines, such as the Ca II IRT, is proportional to the product $Ngf\gamma$ where N is the number density of the absorbing atom or ion, gf is the oscillator strength of the line and γ is the damping parameter. Reliable gf values are known for the IRT lines. In the solar case, a reliable value of the calcium abundance and good state-of-the-art average descriptions of the physical conditions in the atmosphere are available. This allows us to determine with reasonable accuracy the damping parameter γ by varying its value until we obtain a good fit of the relevant line in the observed solar spectrum. In this way Smith & Drake (1988) empirically derived accurate values of the damping constant for collisions with neutral hydrogen from a very careful analysis of center-limb Kitt Peak solar intensity spectra of the IRT lines, using the Holweger-Müller (1974) model atmosphere with the calcium abundance $\log \epsilon_{\odot}(Ca) = 6.36$.

Studies of the Ca II IRT lines in stellar spectra are thus necessarily differential with respect to the Sun. This is why we need to analyse the solar case from good reference solar observations recorded under instrumental conditions as close to the stellar observations as possible. The analysis must be made with a solar model atmosphere consistent with the model atmosphere used for the analysis of the stellar spectra. Scaled solar empirical model atmospheres can be used only in a limited range of stellar atmospheric parameters around those of the Sun. Outside this range, we have to make use of grids of purely theoretical flux-constant model photospheres. Experience shows that the calcium abundance derived from the solar spectrum is somewhat dependent on the choice of the model solar atmosphere (see e.g. Smith 1981). Since $Ngf\gamma$ is the relevant information extracted from the wings of the Ca II IRT, we have to make certain that the damping constants derived from solar observations with different model photospheres are consistent with the calcium abundance corresponding to the particular model photosphere.

4.1. Computations

The computation of the synthetic spectra is carried out by means of the computer code ADRS which is an evolved FORTRAN implementation of the original ALGOL code described by Baschek et al. (1966). This is a fully detailed classical LTE treatment of line formation.

The model atmospheres are also computed in the framework of the LTE theory. A distribution $T(\tau_{\rm ref})$ of the temperature with a reference optical depth scale (here, the monochromatic optical depth at $\lambda = 5000\,$Å) is selected: in general it will be either a scaled solar empirical relation or a relation interpolated in a grid of flux-constant theoretical model photospheres. For a specified chemical composition and surface gravity the continuous opacities are computed and the pressures are obtained by integration of the hydrostatic equilibrium equation in plane-parallel geometry using a separate computer program.

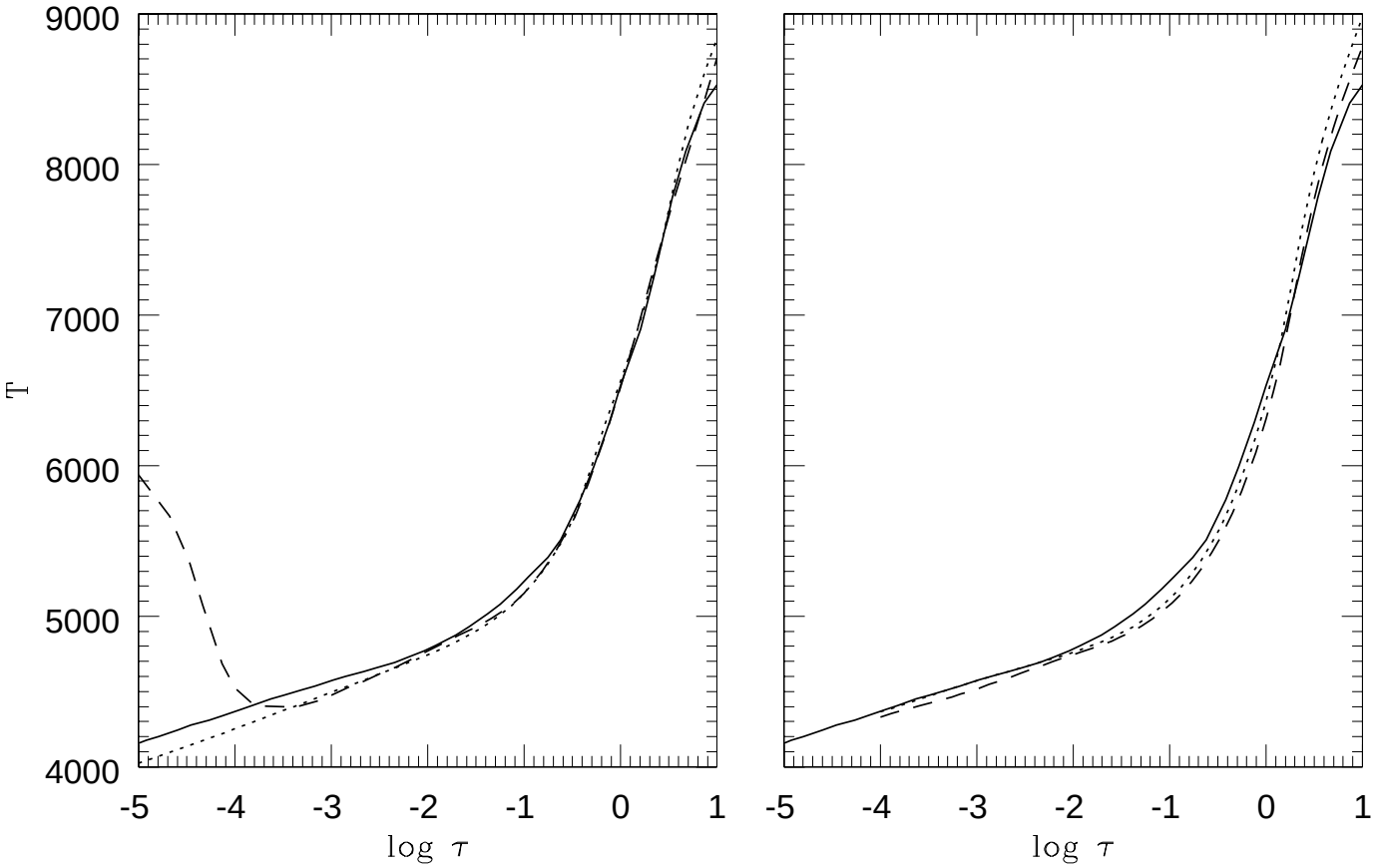

Fig. 3. Comparison of the solar temperature distributions used in this study. The left panel compares the Holweger-Müller model (solid line) with the MACKKL (dashed) and the Kurucz model (dotted). In the right panel the Holweger-Müller model is compared to the GBEN model (dashed) and to the EAGLNT (dotted).

For the solar case I have taken into consideration five different temperature laws (two empirical and three theoretical). The first empirical temperature distribution was that of Holweger & Müller, 1974 (hereafter called Holweger model) which is almost unanimously considered to give the best account of the solar line spectrum in the framework of the LTE theory. Next, the temperature distribution of Maltby et al., 1986 (hereafter MACKKL model) was adopted: it is derived from the very well known empirical laws of Vernazza et al. (1981, VAL models) and includes a more realistic average chromospheric temperature rise. In this special case, as this model incorporates some NLTE features, the original tabulated pressures are used and are not recomputed as stated above. In the category of flux-constant theoretical model photospheres I have chosen the solar model in the grid presented by Eriksson et al. (1979): the models in this grid, which will be subsequently called GBEN models, are computed as described in Gustafsson et al. (1975) and were kindly provided in 1983 by Dr. Eriksson. I have also used the solar theoretical model given in Edvardsson et al. (1993): this model (EAGLNT) is computed basically in the same way as the GBEN models, but using a much more complete line list to account for the line blanketing effects. Finally, I have considered the widely used theoretical solar model atmosphere of Kurucz (1992). These different temperature distributions are compared in Fig. 3. Recent studies that have examined the microturbulence parameter for the Sun-as-a-star full-disk spectrum have found values in the range $0.7 < \xi_t < 1.3\ km\ s^{-1}$ to be appropriate (values of ξ_t for intensity spectra at disk center tend to be smaller and values for intensity at the limb are distinctly larger). A value of $\xi_t = 1.0\ km\ s^{-1}$ has been adopted in this work.

The atomic constants first assumed for the computation of the synthetic spectra are essentially the same as those selected by Smith & Drake (1988) and are summarised in Table 1. The oscillator strengths come from measurements of the lifetime of the upper level and of branching ratios by Gallagher (1967) and are considered to be quite accurate.

As stated before, for such dark lines as the Ca II IRT, the profile depends critically on the damping parameter. In the ADRS code, following Baschek et al. (1966), the damping by collisions with neutral atoms is treated in the classical impact van der Waals approximation. In a van der Waals potential, the frequency shift is given by

$$\Delta\nu = C_{6,\nu}/r^6 \quad \text{or} \quad \Delta\omega = C_{6,\omega}/r^6$$

where C_6 is the interaction constant and r is the interatomic separation. In this approximation, the damping parameter for collisions with neutral hydrogen atoms is

$$\gamma_H = A\, C_6^{2/5} v_H^{3/5} N(HI)$$

Table 1. The atomic constants for the Ca II IRT, after Smith & Drake (1988)

λ	log gf	γ_{rad}	$(\gamma_e/N_e)^*_{5000}$	$(\gamma_H/N_H)^\dagger_{5000}$
8498.02	-1.45 ± 0.05	1.5×10^{-8}	3.0×10^{-6}	$(2.14 \pm 0.10) \times 10^{-8}$
8542.09	-0.50 ± 0.05	1.5×10^{-8}	3.0×10^{-6}	$(2.06 \pm 0.10) \times 10^{-8}$
8662.14	-0.76 ± 0.05	1.5×10^{-8}	3.0×10^{-6}	$(2.00 \pm 0.10) \times 10^{-8}$

$* \; T^{1/6}$ dependence;
$\dagger \; T^{0.4}$ dependence

where A is a numerical constant, $N(HI)$ is the number density of the perturbing particles (here, neutral hydrogen) and v_H is the relative velocity of the perturbing atom, $v_H \approx (8kT/\pi m_H)^{1/2}$, in such a way that $\gamma_H/N_H \propto T^{0.3}$. This is expressed numerically, in c.g.s. units ($rad\ s^{-1}\ cm^3$) as

$$\log(\gamma_H/N_H) = 3.4053 + 0.3 \log T + 0.4 \log C_{6,\omega}$$

Data on the interaction constant are not always available in the literature: in that case, it is often estimated from an approximate hydrogen-like formula ("Unsöld's formula"), multiplied by an arbitrary (adjustable) enhancement factor which will generally take a value between 1 and 5 (see in Fig. 8 a synthetic profile computed with the damping parameter predicted by Unsöld's formula, with unit enhancement factor).

The contribution of the collisions with neutral helium is accounted for by multiplying γ_H by a factor

$$1 + (p_{He}/p_H)^{2/5} (\mu_H/\mu_{He})^{3/10} (N(He)/N(HI))$$

where p is the polarisability and μ the atomic weight.

Attention must be paid to some confusion in the literature concerning the symbols used. The interaction constant is usually refered to as C_6 and it is often not immediately clear, even from the context, whether $C_{6,\nu}$ or $C_{6,\omega}$ is meant. In many papers or textbooks the damping constant γ is the full width at half maximum (FWHM) of the Lorentzien profile of the absorption coefficient; but other authors, among which are G. Smith and collaborators, refer to γ as being the half width at half maximum. Here, γ will refer to the FWHM. These choices affect the value which must be used for the numerical constant A.

There is, however, evidence from both experimental and theoretical work, that the treatment based on pure van der Waals interaction is inadequate and leads to systematic underestimates of the damping constant. At high stellar photospheric temperatures it turns out that short-range repulsive forces largely dominate the broadening interactions (see e.g. O'Neill & Smith, 1980). These are often successfully described in the classical impact approximation by adding an r^{-12} repulsive term to the interaction potential. All the recent developments point toward a $T^{0.4}$ temperature dependence of the damping constant instead of the $T^{0.3}$ expected for pure van der Waals interaction. For these reasons, following G. Smith and collaborators, I modified the ADRS code to allow optional treatment of the damping by collisions with neutral hydrogen atoms according to:

$$\gamma_H/N_H = (\gamma_H/N_H)_{5000}\ (T/5000)^s$$

where the damping coefficient per unit perturber at $T = 5000\,K$, $(\gamma_H/N_H)_{5000}$, and the exponent s are the input parameters. The pure van der Waals case is recovered with $s = 0.3$ and

$$\log\ (\gamma_H/N_H)_{5000} = 4.515 + 0.4 \log C_{6,\omega}$$

From numerical experiments involving computations of the Ca II IRT lines with several model atmospheres for different effective temperatures, it turned out that *lines synthetised with an identical value of* $(\gamma_H/N_H)_{5000}$ *at* $T = 5000\,K$*, but either a* $T^{0.4}$ *or a* $T^{0.3}$ *dependence, gave indistinguishable profiles.* Nevertheless, the synthetic profiles described hereafter were all computed assuming the more physical $s = 0.4$.

The radiative damping and electron Stark broadening are also treated in the same way as in Smith & Drake (1988). The radiative damping parameter is safely derived from the lifetime of the upper levels, the lower levels being metastable. The Stark broadening by collisions with electrons is treated in the classical impact approximation with a $T^{1/6}$ dependence and a damping constant based on measurements by Chapelle & Sahal-Bréchot (1970). Similar relations hold as in the van der Waals case, with an interaction constant $C_{4,\omega}$, in such a way that

$$\log\ (\gamma_e/N_e) = \log\ (\gamma_e/N_e)_{5000} + \frac{1}{6} \log\ (T/5000)$$

$$\log\ (\gamma_e/N_e) = 2.9875 + \frac{1}{6} \log T + \frac{2}{3} \log C_{4,\omega}$$

with

$$\log\ (\gamma_e/N_e)_{5000} = 3.6040 + \frac{2}{3} \log C_{4,\omega}$$

Before being compared with the observed spectrum, the synthetic spectra have to be convolved with different macroscopic broadening profiles. On our CFH solar observations, the spectrograph's instrumental profile appears to dominate the macro-broadening contributions. Other contributions come from macroturbulence (width $\sim v_G^\odot \approx 2\ km\ s^{-1}$) or rotation ($v_{rot}^\odot \approx 1.8\ km\ s^{-1}$). At the resolution of typical CFH stellar spectra, numerous synthetic spectrum calculations in the solar case have shown that the global macro-broadening processes can adequately be represented by a unique convolution with a gaussian profile, the width of which, v_G, may be adjusted so as to reproduce as well as possible the observed breadth of well defined unblended weak atomic lines lying in the observed spectral region. In the present case, the only really adequate lines for that purpose are the Fe I lines at $\lambda 8514.08$ and $\lambda 8515.12$ Å. Best-fitting synthetic profiles are obtained with the convolution by a gaussian profile having a characterestic width

$v_G = 6.3 \pm 0.1\ km\ s^{-1}$. This result does not depend on the adopted model atmosphere and a change in the adopted microturbulence from $\xi_t = 1.0$ to $1.3\ km\ s^{-1}$ does not change v_G by more than $0.05\ km\ s^{-1}$. Should we have to deal with a star with appreciable rotation, this would have to be taken explicitely into account because the rotational broadening is rather elliptical, far from gaussian. In the same way, when the synthetic spectra are to be compared with the Solar Flux Atlas, we find that the combined effects of macroturbulence and instrumental broadening are well represented by convoluting the computed flux profiles by a gaussian of width $v_G = 2.18\ km\ s^{-1}$.

It turned out that the synthetic profiles of the very broad Ca II IRT lines are rather insensitive to the precise values adopted for the instrumental, Stark damping, micro- or macro-turbulence broadening parameters. They are however, as expected, quite sensitive to the calcium abundance and to the value of the hydrogen damping parameter γ_H.

4.2. Solar calcium abundance

When interpreting spectra, we generally use temperature distributions interpolated in the GBEN grid of flux-constant model atmospheres. Preliminary computations of the Ca II IRT profiles were carried out using the "canonical" calcium abundance $\log \epsilon_\odot(Ca) = 6.36$ and the values of the damping parameter provided by Smith & Drake (1988). The synthetic profiles calculated with the Holweger-Müller temperature distribution correctly matched the observed profile, but those calculated using the GBEN solar model atmosphere produced quite unsatisfactory results: the computed wings of the IRT lines were much too deep compared with the observed profiles. This evidently resulted from assuming a calcium abundance which was not consistent with the choice of the model temperature distribution. Therefore, the calcium abundance must first be redetermined for each of the selected model atmospheres. To that purpose the Ca I lines equivalent widths (for intensities at the center of the solar disk) listed in Table 1 of Smith (1981) were used. A number of lines considered as discrepant by the author were discarded, as well as the lines with equivalent widths $W_\lambda > 125$ mÅ, reducing the number of "useful" Ca I lines to 14. Most of these lines are of medium strength so that their equivalent width is sensitive to the adopted damping and microturbulence parameters. Good estimates of the oscillator strengths and damping parameters are given by Smith (1981). For each solar model atmosphere the value of the microturbulence (assumed to be constant with depth) was adjusted to cancel any systematic dependence on the equivalent width of the individual abundances derived from each line. The resulting average values of the calcium abundance and of the microturbulence ξ_t are given in Table 2. Let us remark that if, with the Holweger-Müller model, we use "default" damping parameters calculated from Unsöld's formula with a unit enhancement factor (as often done in abundance studies), we obtain $\log \epsilon_\odot(Ca) = 6.46 \pm 0.08$ and $\xi_t = 0.75 \pm 0.40\ km\ s^{-1}$, i.e. values which are appreciably different from the values listed in Table 2. As already observed by Smith (1981) we see that the calcium abundance is somewhat dependant on the choice of the model atmosphere. The value obtained for the abundance with the Holweger model is slightly higher (0.02 dex) than that given by Smith; this probably comes from using somewhat higher continuous opacities and a reduced line list.

4.3. Perturbation by hydrogen Paschen lines

The Ca II IRT lines are generally considered to be a useful diagnostic tool in the range of late F to M stars. Hydrogen Paschen lines happen to fall in the red wings of the CaII IRT lines and start to contribute significantly at the hotter end of this range: P16 $\lambda 8502.49$ lies in the wing of Ca II $\lambda 8498.02$, P15 $\lambda 8545.39$ falls in that of Ca II $\lambda 8542.09$ and P13 $\lambda 8665.02$ blends with Ca II $\lambda 8662.14$. In the hotter stars, the Paschen lines dominate the Ca II lines: this is quite well illustrated by Fig. 1 of Ginestet et al. (1994) which shows this spectral region in A5 stars of different luminosities. The little perturbed P14 $\lambda 8598.39$ line falls in between the two strongest Ca II lines: it thus allows to estimate the importance of the perturbation of the Ca II IRT by the hydrogen Paschen lines. Inspection of the Atlas of Carquillat et al. (1997) shows that P14 is readily identified in stars as cool as G0, with a strong positive luminosity effect. Therefore, the contribution of the Paschen lines must be taken into account for the quantitative interpretation of the Ca II IRT line wings in stars earlier than the Sun.

In the solar case, Smith & Drake (1988) argue, on the basis of the non-detection of P14, that the hydrogen contribution to the observed profiles of the Ca II IRT lines is negligible. And, indeed, synthetic profiles fitting the observed blue wing of $\lambda 8498$ or $\lambda 8542$ do not leave room for a significant additional absorption in the red wing. Only does the $\lambda 8662$ line show a slight, but significant, extra absorption in the red wing which can be attributed to P13.

R. and G. Cayrel, and collaborators, use the outer profile of the Balmer H_α line as a temperature criterion. For that purpose they compute synthetic Balmer line profiles with the help of an LTE computer code initially written by Praderie (1967), and later updated and implemented by R. Cayrel, A. Talavera and M. Spite. This computer program, called HYDRO, also computes profiles of the Paschen lines. I have used it to try and assess more quantitatively the contribution of the Paschen line absorption to the Ca II IRT line profiles in the Sun and hotter stars. The optical depths in the Paschen lines at selected frequencies, as computed by program HYDRO, are written to a file. Monochromatic line optical depths from the several Paschen lines that can contribute are separately summed up; components with central wavelengths distant by more than $\Delta\lambda = 35$ Å from the current frequency point are extrapolated according to a $\Delta\lambda^{-5/2}$ law. The spectrum synthesis program ADRS has been modified to read the file of the total Paschen line optical depths and add them to the total computed (continuous plus other lines) optical depths.

Synthetic Ca II $\lambda 8498$ and $\lambda 8542$ profiles have been computed taking into account the total contribution of P14 through P17. In the solar case, as illustrated by Fig. 2, the profiles computed with the Holweger model show only a very slight red wing

Table 2. Calcium abundance, microturbulence and hydrogen damping parameters derived with the five solar model atmospheres considered.

λ	Model	Holweger	MACKKL	EAGLNT	GBEN	Kurucz
	$\log \epsilon(Ca)$	6.38 ± 0.02	6.34 ± 0.02	6.27 ± 0.03	6.25 ± 0.03	6.34 ± 0.02
	$\xi_t\ [km\ s^{-1}]$	1.17 ± 0.10	1.09 ± 0.07	1.08 ± 0.13	1.10 ± 0.13	1.06 ± 0.07
	$(\gamma_H/N_H)_{5000} \times 10^8$	1.95 ± 0.05	1.95 ± 0.05	2.11 ± 0.08	2.26 ± 0.16	1.82 ± 0.08
8498	$\log C_{6,\omega}$	-30.560	-30.560	-30.478	-30.405	-30.640
	E_6	10.5	10.5	12.7	15.1	8.77
	δ	0.026	-0.003	0.054	0.124	-0.072
	$(\gamma_H/N_H)_{5000} \times 10^8$	1.89 ± 0.05	1.91 ± 0.04	2.05 ± 0.08	2.17 ± 0.15	1.80 ± 0.07
8542	$\log C_{6,\omega}$	-30.595	-30.585	-30.510	-30.447	-30.650
	E_6	9.75	9.98	11.9	13.7	8.59
	δ	0.028	0.014	0.058	0.120	-0.055

asymmetry, and the main effect of the Paschen lines absorption is to lower significantly the apparent continuum location. Thus, as explained in Sect. 3.2, solar spectra observed under "stellar" conditions (over rather short wavelength ranges) must be locally renormalized to ensure consistency in the comparison between computed and observed profiles. We can indeed check that the renormalized continuum of our CFH spectrum coincides with the Solar Flux Atlas definition (which is based on consideration of very long wavelength scans) if and only if we take explicitly the Paschen lines into account in the calculations. This demonstrates the validity of our renormalization procedure and shows that the computed flux in the far wings of the Paschen lines is correct. According to the Eddington-Barbier approximation the intensity at disk center reflects the value of the source function at total optical depth $\tau_t = 1$ and the measured flux is typical of the value of the source function at $\tau_t = \frac{2}{3}$. One finds that the Paschen lines, at the central wavelength of P15, contribute to the total optical depth τ_t by only 1.2% at $\tau_t = 1$ and 0.9% at $\tau_t = \frac{2}{3}$. The maximum contribution of the Paschen absorption at $\tau_t = 1$ in the $\lambda 8542$ line wing is 1.6% at $\lambda 8546.8$; at $\tau_t = \frac{2}{3}$ the corresponding maximum is 1.0% at $\lambda 8546.2$. We thus see that, in the solar case, the contribution of the Paschen lines to the Ca II IRT features is almost negligible. Their effect is essentially the same as that of a slight increase of the continuous absorption coefficient.

We shall see, however, in Sect. 5.1, that the hydrogen absorption is no longer negligible for stars hotter and/or more luminous than the Sun (see Table 3). This must be taken into account when calculating synthetic profiles as well as for the continuum normalization.

4.4. Solar synthetic spectra

Synthetic profiles of the first two Ca II IRT lines, $\lambda 8498$ and $\lambda 8542$, were computed with each of the five selected solar model atmospheres, with due account for Paschen line absorption. For each model, the value of the hydrogen damping parameter γ_H of each line was changed until a "best possible fit" of the observed solar profile was obtained. This raises the question of the choice of "best fitting" criteria. As already stated, the central core of the IRT lines is formed under conditions departing from LTE and, thus, it is not expected to be correctly represented by LTE synthetic profiles. These criteria must therefore be restricted to the outer wings which are formed in layers where LTE prevails, i.e., as experience shows, that part of the wings where the depression in the profile, $D_\lambda = 1 - F_\lambda/F_c$, is smaller than $D_\lambda \approx 0.32$ (see the following discussion of the fits obtained with the Holweger or MACKKL empirical model atmospheres). For accurate fits, another difficulty comes from the slight asymmetries of the observed profiles: it is clear that the cores are somewhat red-shifted relative to the wings and that the bisectors of each profile at different depressions do not fall at exactly the same wavelength. The synthetic profiles, computed for basically static model atmospheres, are unable to reproduce these asymmetries. This makes it difficult to compare observed with computed depressions at an exact given wavelength. Uncertainties in the wavelength calibration of the observations and in the radial velocity shift of the star add to this difficulty. Alternatively, if we assume that the radiation on either side of the line center at a given depression is formed in the same layers (with the same motions) the comparison between the observed and computed line *widths* at selected values of the depression is not affected by these uncertainties. This method has been chosen here. For the empirical determination of γ_H the synthetic profiles were primarily compared with the quasi-noiseless Solar Flux Atlas. The selected values of the line depression are $D_\lambda =$ 0.185, 0.21, 0.24, 0.28 and 0.31 for $\lambda 8498$, and $D_\lambda = 0.175$, 0.19, 0.22, 0.30 for $\lambda 8542$. In the special case of the $\lambda 8498$ feature a correct representation can only be obtained by taking also into account the blending Fe I line at $\lambda = 8496.99$ Å; the gf value of the Fe I line is adjusted so as to reproduce the observed value of its central depth.

The "best fit" $(\gamma_H/N_H)_{5000}$ values found in this way are shown in Table 2. They are averages of the values fitting the profile width at each selected line depression; the rms uncertainties quoted in the table come from the dispersion of the values of the damping constant derived at each of the selected depressions (only an ideal fit would produce a unique value of $(\gamma_H/N_H)_{5000}$ at each of them). Thus the values in Table 2 reflect best fits in a range of depressions restricted to $0.18 \leq D_\lambda \leq 0.30$, which means that the quoted uncertainties are consistently underevaluated. Let $\Gamma(D_\lambda)$ be the value of $(\gamma_H/N_H)_{5000}$ such that the

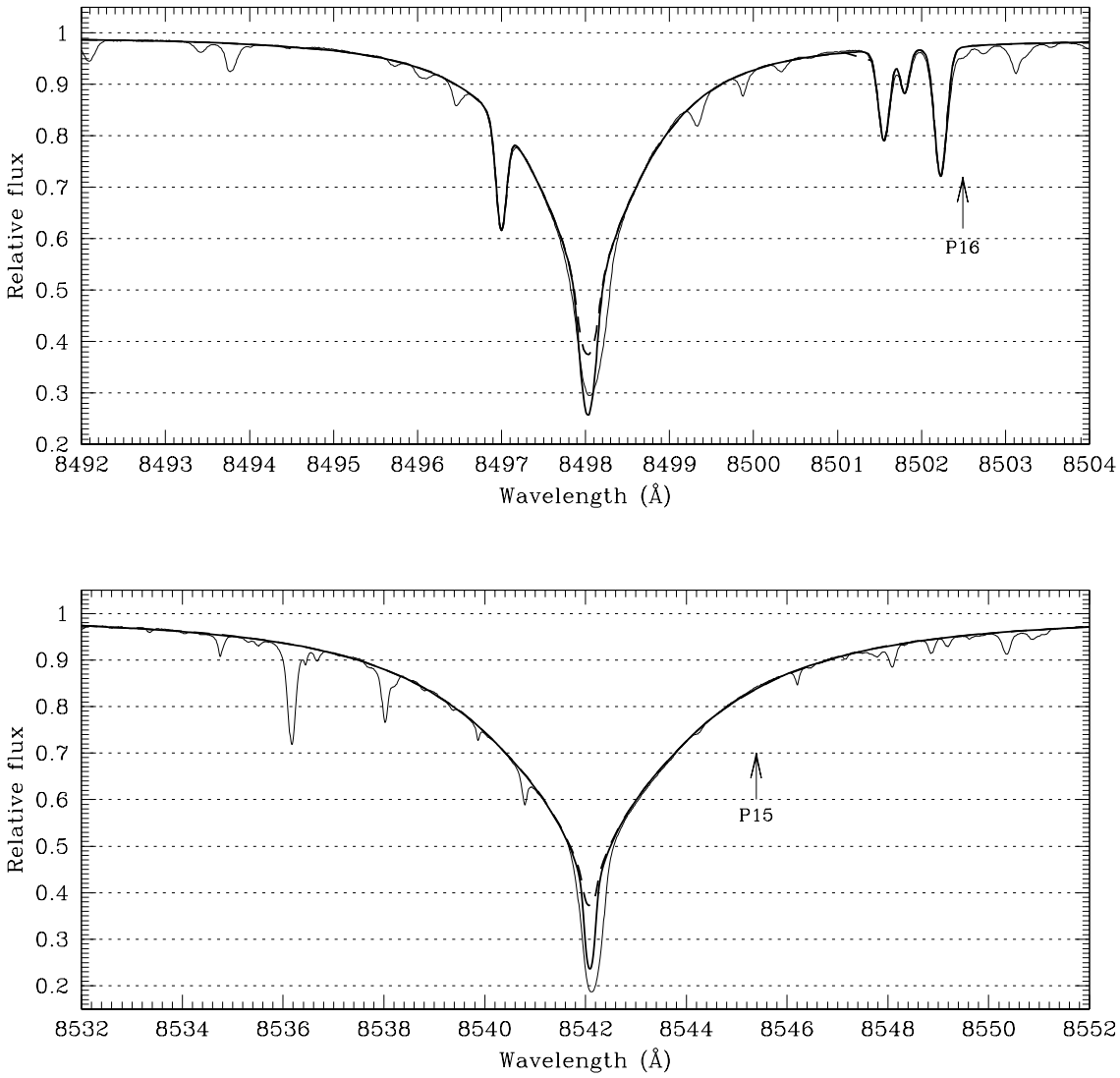

Fig. 4. Synthetic spectra computed with the Holweger model. Thin solid line: observed spectrum. Thick solid line: profile computed with the full Holweger model. Dashed line: profile computed with a Holweger model truncated upwards at $\tau_{0.5} = 10^{-4}$. The location of the center of perturbing Paschen lines is indicated by arrows.

width of the computed profile at the depression D_λ is equal to the observed value. In general the actual fits tend to imply a clear monotonous trend of $\Gamma(D_\lambda)$ with D_λ. Accordingly, a measure of the quality of the fit may be given as, for example, the relative difference $\delta = 2[(\Gamma(0.3) - \Gamma(0.2))/(\Gamma(0.3) + \Gamma(0.2))]$. The relative difference δ is given in Table 2 for each of the adopted model atmospheres.

4.4.1. Holweger-Müller model

The synthetic spectra (thick solid lines) obtained with the Holweger model are illustrated in Fig. 4 for the first two IRT lines and are compared with the observed profiles (Solar Flux Atlas - thin lines). The synthetic spectra quite accurately represent the observed profiles in the line wings, at distances from the line center $|\Delta\lambda| > 0.55$ Å for the $\lambda 8498$ Å line, and $|\Delta\lambda| > 1.05$ Å for the $\lambda 8542$ Å line, i.e. respectively $D_\lambda < 0.31$ and $D_\lambda < 0.35$. As expected, the line cores are not adequately represented by these LTE computations. In both lines the observed line core is broader and slightly red-shifted relative to the computed core. Curiously the observed core is less deep than computed for the $\lambda 8498$ line, whereas it is deeper in the case of the $\lambda 8542$ line. The latter behaviour is indicative of a source function ruled by diffusion processes; the apparently different behaviour of the $\lambda 8498$ line may be explained by a more effective filling in by chromospheric emission in conformity with what was observed by Shine & Linsky (1972) on spectra of solar plages of different degrees of activity. The greater reactivity of $\lambda 8498$ to the degree of activity is not easy to explain: to account for it, Shine & Linsky (1974) must play with the temperature distribution in the chromosphere, the depth distribution of microvelocities and the effect of macrovelocities.

These LTE computations show that the center of the two lines is completely opaque already at the surface of the model

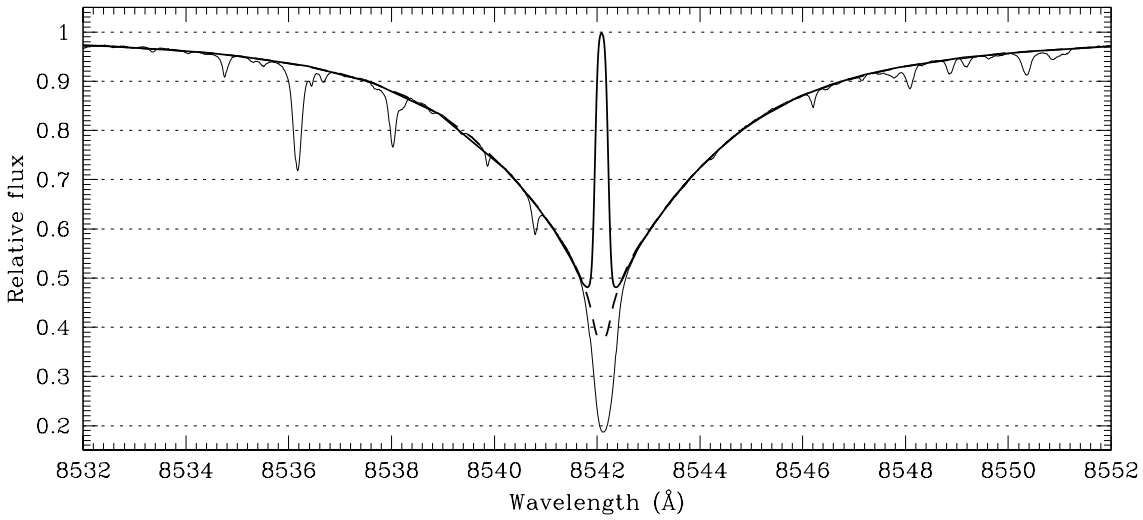

Fig. 5. Synthetic profiles computed with the MACKKL model. Thick solid line: full model, with chromosphere; dashed line: photospheric part of the MACKKL model only, starting at $\tau_{0.5} = 10^{-4}$. The thin line shows the observed profile.

atmosphere. The solar model atmosphere given by Holweger & Müller (1974) starts at the reference optical depth (monochromatic optical depth at 0.5 μ) $\tau_{0.5} = 3 \times 10^{-7}$. Experimenting with a model extrapolated upwards, we find that, in LTE, the total optical depth at line center is unity at $\tau_{0.5} = 1.07 \times 10^{-6}$ for $\lambda 8498$, and $\tau_{0.5} = 8.89 \times 10^{-8}$ for $\lambda 8542$. In LTE, the intensity at the line center is thus fixed by the Planck function at the temperature of the uppermost layer, and, therefore, depends on the "starting" (uppermost) reference optical depth of the model atmosphere. The Holweger model is constructed empirically and aims at reproducing as well as possible the continuum and line data of the observed solar spectrum in the visible and near infrared; it does not feature a chromospheric temperature rise and, although it extends up to $\tau_{0.5} = 3 \times 10^{-7}$ it is not considered to be physically meaningful above $\tau_{0.5} \simeq 10^{-4}$ where the actual chromospheric temperature rise occurs. Most theoretical flux-constant model photospheres usually start at $\tau_{0.5} \geq 10^{-4}$ and do not include chromospheric layers. If we want to compare results obtained by means of the Holweger model with results produced by means of some theoretical photosphere, we should use a version of the Holweger model for which the layers above $\tau_{0.5} = 10^{-4}$ have been cut away. In Fig. 4 the profiles computed using such a "truncated" Holweger photosphere are represented by dashed lines. They depart significantly from the profiles computed with the full Holweger model only in the very central core, within $|\Delta\lambda| < 0.31$ Å from the center of $\lambda 8498$ and $|\Delta\lambda| < 0.44$ Å for $\lambda 8542$. This demonstrates that these central regions of the Ca II lines are indeed formed in chromospheric layers.

Synthetic profiles have also been computed with the Holweger model in the van der Waals damping approximation, with the same value of γ_H/N_H at the reference temperature of 5000 K, but a $T^{0.3}$ instead of a $T^{0.4}$ dependence. They turn out to be indistinguishable from the profiles discussed above. Therefore the IRT lines can be correctly described with the more commonly used van der Waals approximation. The corresponding interaction constant $C_{6,\omega}$ (see the correspondence formula in Sect. 4.1) is given in Table 2, as well as the enhancement factor E_6 of $C_{6,\omega}$ relative to the Unsöld approximation. We see that this factor is unusually high for the Ca II IRT.

4.4.2. MACKKL model

The MACKKL model (Maltby et al., 1986) is an empirical model of the average solar atmosphere which includes a chromospheric temperature rise starting at $\tau_{0.5} = 2.5 \times 10^{-4}$, upwards to $\tau_{0.5} = 4.3 \times 10^{-9}$. The computed and observed profiles of the $\lambda 8542$ line are compared in Fig. 5. The thin solid line shows the observed spectrum and the thick solid line shows the profile computed by means of the full MACKKL atmosphere; again, the dashed line shows the profile computed by means of a MACKKL model starting at $\tau_{0.5} = 10^{-4}$ and consisting only of its photospheric part (temperature increasing monotonically with optical depth).

As expected in LTE, the chromospheric temperature rise results in a strong emission peak in the core of the computed profile. But, as already shown by, e.g., Shine & Linsky (1974) or Jørgensen et al. (1992), the LTE approximation is not expected to be valid in the core of the IRT lines. The value of the test-parameter δ indicates, however, that the fit to the observed line wings is good and even better than with the Holweger model. The comparison between the observed and computed profiles basically confirms the conclusions drawn in the case of the Holweger model, i.e. that the core of the line, within $\Delta\lambda = \pm 0.45$ Å, is formed in the chromosphere under conditions strongly deviating from LTE. Outside this interval the good quality of the fit to the observed profile strongly suggests that the line wings are formed in the photosphere under conditions very close to LTE. The case of the $\lambda 8498$ line, which will not be shown here, is exactly similar to that of $\lambda 8542$ and confirms the discussion given above. Even though the calcium abundances derived with the Holweger and the MACKKL mod-

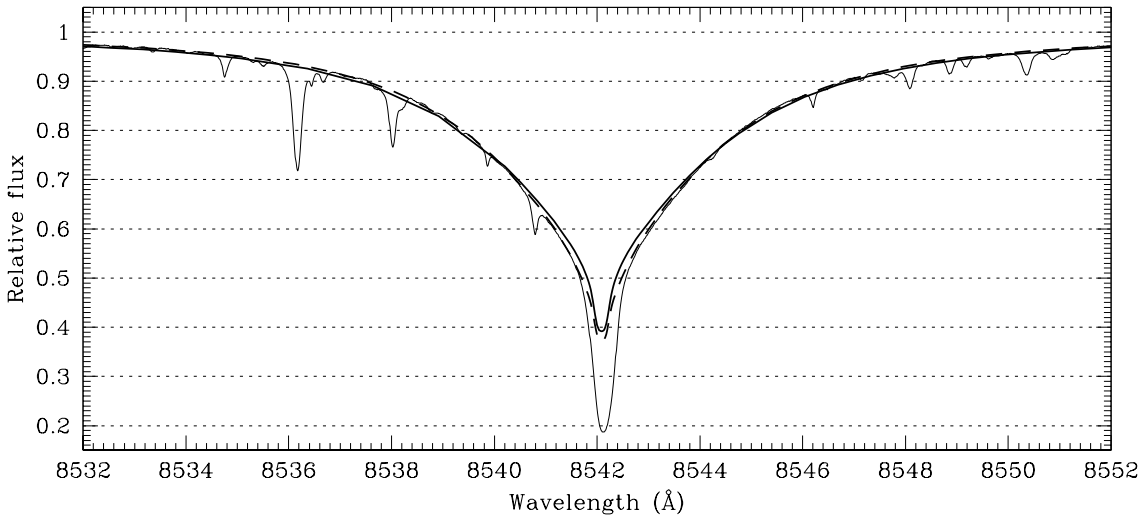

Fig. 6. Synthetic profile computed with the GBEN model (thick solid line). The observed spectrum is drawn as a thin continuous line. For comparison the profile computed with the Holweger model starting at $\tau_{0.5} = 10^{-4}$ is superimposed as a broken line.

els are slightly different, the hydrogen damping constants derived with both models are quasi identical.

4.4.3. GBEN theoretical model

The fit to the observed line wings obtained with the theoretical flux-constant GBEN model photosphere (Eriksson et al. 1979, Gustafsson et al. 1975) is much less satisfactory, as illustrated by a much higher value of the test-parameter δ. The "best fit" synthetic profile of the $\lambda 8542$ line computed with the GBEN model and the corresponding damping parameter given in Table 2 is shown in Fig. 6. It can be seen that while the predicted profile has the same width as the observed one at $D_\lambda = 0.27$, it is clearly too broad for $D_\lambda < 0.20$ and too narrow for $D_\lambda > 0.30$. It is still possible to give an average value of the damping parameter, but with somewhat larger error bounds. In that respect, and within the accuracies typical of fine analyses (see Sect. 4.4.6), the empirical model temperature distributions give more adequate results than the theoretical flux conxtant GBEN temperature distribution. Synthetic profiles for the $\lambda 8498$ line present exactly the same problems as for $\lambda 8542$.

4.4.4. EAGLNT theoretical model

The extensive study by Edvardsson et al. (1993) of the abundances of the elements in 189 F and G dwarfs is based on a grid of theoretical model photospheres which is basically an improvement of the GBEN grid. They are computed with essentially the same computer code but using a more complete line list to account for the line blanketing effects. The solar model of this new grid (Table 6 of their paper) has been used to compute synthetic profiles of the Ca II IRT lines and the result for the $\lambda 8542$ line is shown in Fig. 7. As shown by the value of the test-parameter δ, they provide a much better match of the observed profiles than that obtained with the GBEN model, although the quality of the fit is not yet as good as with the empirical models. The extended line list of Edvardsson et al. thus leads to significantly improved photospheric temperature distributions.

4.4.5. Kurucz theoretical model

With the preceding theoretical model atmospheres, when γ_H is chosen to match exactly the width of the observed profiles at a depression D_λ of, say 0.22, the predicted profiles are too narrow at deeper depressions ($D_\lambda > 0.22$). As seen in Fig. 8, the opposite is true of profiles obtained with the Kurucz (1992) solar model photosphere: the predicted widths are somewhat too wide at the deeper depressions, resulting in a negative value of δ. Thus, in the LTE approximation, the Kurucz model does not allow as good a representation of the Ca II IRT lines as that obtained with the empirical models. The absolute value of δ shows that the $\lambda 8542$ line is as correctly represented with the Kurucz model atmosphere as with the EAGLNT; for the $\lambda 8498$ line, however, the Kurucz model fares substantially worse than the EAGLNT.

4.4.6. Comparison with the CFH solar profiles

The same fitting procedures have also been carried out, but comparing, this time, the synthetic profiles computed with the different model atmospheres to the properly renormalized "stellar quality" CFH solar spectrum instead of the Solar Flux Atlas. The fits obtained have the same quality as the previous ones and the values derived for γ_H are consistent with those found in Table 2, although with a slightly higher uncertainty (by less than $\approx 0.03 \times 10^{-8}$) due to the non-negligible noise in the CFH data ($S/N \approx 200$). In the presence of noise, at each depression D_λ, $\Gamma(D_\lambda)$ is affected by a certain uncertainty. When interpreting stellar spectra, if the derived $\Gamma(D_\lambda)$'s are equal within their error bars on the selected range of $0.18 < D_\lambda < 0.31$, we will consider that a given model provides a satisfactory representation of the Ca II IRT. From this point of view, when the synthetic

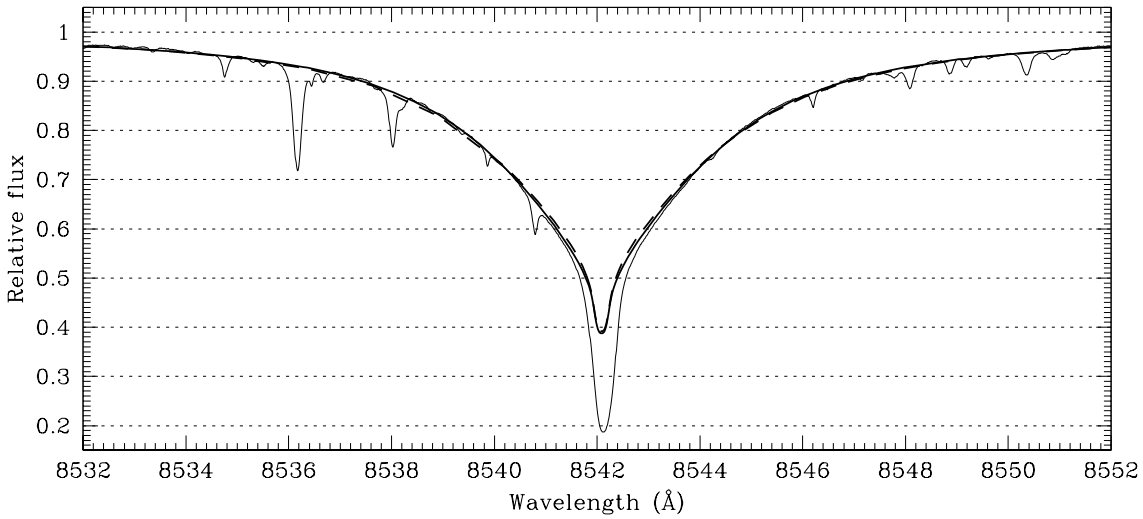

Fig. 7. Synthetic profile computed with the EAGLNT model (thick line). The profile computed with the GBEN (dashed line) is shown for comparison. The observed profile is represented by the thin line.

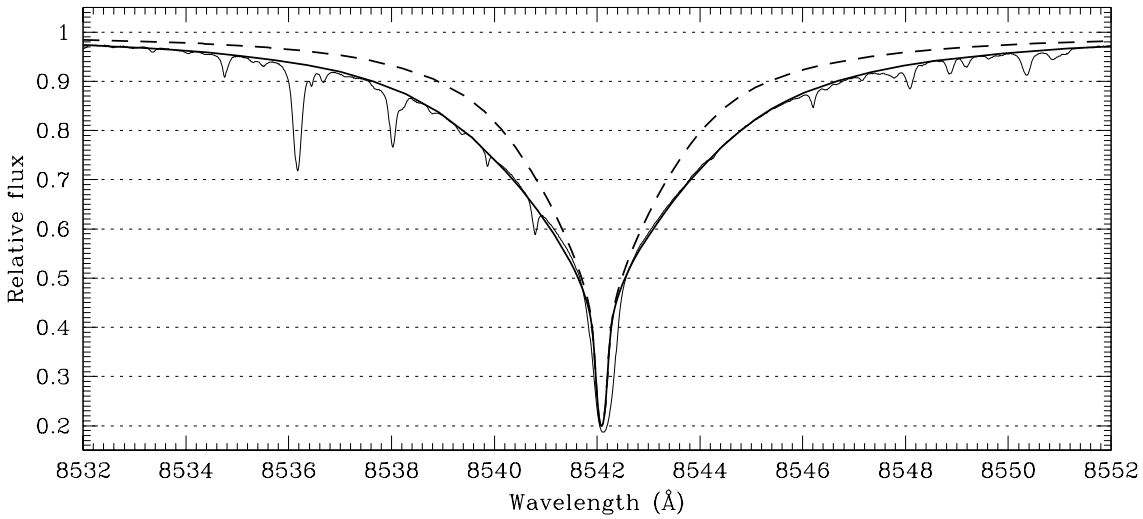

Fig. 8. Synthetic profile computed with the Kurucz model. For illustration purposes the dashed line shows a synthetic profile calculated with the Kurucz model and the van der Waals interaction constant in the Unsöld approximation, with unit enhancement factor.

profiles described above are compared with the CFH spectrum, the Holweger, MACKKL and Edvardsson models qualify as sufficiently adequate models of the solar atmosphere, whereas the GBEN and Kurucz models don't.

Other computations have also been made, neglecting the Paschen lines contribution. If a self-consistent treatment of the continuum normalization is carried out, they lead to $(\gamma_H/N_H)_{5000}$ values only slightly smaller than those in Table 2 (by $\approx 0.07 \times 10^{-8}$, which is about the size of the uncertainties).

4.4.7. Conclusions of the solar computations

In summary, we confirm that the derived calcium abundance as well as the interaction constants for broadening by collisions with neutral hydrogen atoms depend somewhat on the model photosphere used for the computations. The consequence is that, if we want to analyse stellar spectra of the Ca II IRT lines differentially with respect to the Sun, we need to refer to the abundance and hydrogen damping constants determined in the solar case by means of a solar model atmosphere consistent with the model atmospheres used for the program stars. The very low uncertainties on the solar calcium abundance quoted in Table 2 refer only to uncertainties in the line atomic parameters and equivalent width measurements. In an effort to include the contribution of the choice of the model atmosphere to the uncertainties, we may restrict ourselves to averaging the results obtained with the Holweger, MACKKL and EAGLNT models (the only ones correctly describing the CFH observation), which leads us to recommend the following value for the solar calcium abundance $\log \epsilon_{\odot}(Ca) = 6.33 \pm 0.06$, and, for the hydrogen damping constants: $(\gamma_H/N_H)_{5000} = (2.00 \pm 0.11) \times 10^{-8}$ for $\lambda 8498$ and $(\gamma_H/N_H)_{5000} = (1.95 \pm 0.10) \times 10^{-8}$ for $\lambda 8542$.

Within the error limits, these values are consistent with the damping constants obtained by Smith & Drake (1988) from very high quality solar intensity spectra, using the Holweger-Müller model atmosphere.

5. Sensitivity to the atmospheric parameters

As summarized in Sect. 2, the sensitivity of the Ca II infrared triplet lines to changes in the basic stellar atmospheric parameters has already been investigated in a number of papers. Several of them refer to integrated widths which are not fully descriptive and easy to interpret in the context of high resolution profile studies. None of the papers based on a theoretical approach take the effect of Paschen lines absorption into account, which becomes an important factor at higher temperatures or lower luminosities. In the following pages, an attempt is made to illustrate the response of the profile of the strongest $\lambda 8542$ line to changes in the atmospheric parameters. To this end I have computed synthetic profiles of that line for a set of model atmospheres extracted from a homogeneous grid. For mid-F to K stars, such a homogeneous grid of model stellar photospheres is provided by the GBEN grid (Gustafsson et al. 1975, Bell et al. 1976, Eriksson et al. 1979). The discussion in Sect. 4 has shown that it was possible to obtain a good fit of the observed wing profiles of the Ca II IRT in the solar flux spectrum by LTE computations carried out with adequate empirical model solar photospheres. This tends to indicate that our physical description of the conditions of formation of these lines is essentially correct. Thus, even though the fit obtained with the solar model of the GBEN grid is not perfect, we expect that the differential variations of the computed profiles with changes in the basic model parameters will be adequately described, at least to first order, if we use model photospheres interpolated in the homogeneous GBEN grid.

The computations were carried out in exactly the same conditions as in the solar case. The emergent theoretical profiles were broadened by a gaussian profile with a width of $6.3\,kms^{-1}$ to mimic a typical stellar profile observed with a standard high resolution coudé spectrograph. The Paschen lines absorption was taken explicitely into account in all cases.

Subsequently, the response of the computed line profiles will be illustrated by figures showing how the full profile changes when only one of the three basic atmospheric parameters (effective temperature, gravity or metallicity) is changed at a time. It will be apparent that the development of the LTE part of the profiles can be characterized by changes in the depression at the wavelengths $\lambda = 8539$ and $\lambda = 8545$ Å which fall in regions which, at the same time, are well described in the LTE approximation and are not affected by telluric absorption features. At $\lambda = 8539$ Å the depression is little affected by the Paschen lines, whereas the perturbation is nearly maximal at $\lambda = 8545$ Å.

5.1. Contribution of the Paschen lines

Table 3 shows the relative contribution of the Paschen lines in the region of formation of the observed intensity at the center of the disk (unit total optical depth) in the red wing of the Ca II $\lambda 8542$ line. For the formation of the flux (at $\tau_{tot} \approx \frac{2}{3}$) the contribution is, on average, 80% of that given in Table 3. What is most striking in this table is the very strong positive luminosity effect on the contribution of the hydrogen lines. As can be anticipated, there is also a metallicity effect, although much weaker, in the sense of metal-poor stars showing a larger hydrogen contribution than more metal-rich stars. The assumptions on which the calculations are based (LTE and plane-parallel geometry) may loose their validity for the most luminous stars, but these clear trends will still prevail.

Table 3. Percent contribution of the Paschen lines to the total optical depth at $\tau_{tot} = 1$, near the center of the P15 line $(\lambda 8545.39)$.

[M/H]	$\log g$	$T_{\rm eff}$	C [%]
0.	4.5	6500	6.7
		6250	3.7
		6000	1.8
		≤ 5750	≤ 1.0
	3.0	6000	12.6
		5500	2.9
		5000	0.4
	1.5	6000	34.0
		5500	9.5
		5000	1.6
-0.5	4.5	6000	2.4
-1.0	4.5	6000	3.4
		5500	0.8

5.2. Sensitivity to the effective temperature

Fig. 9 shows predicted profiles for solar composition dwarf stars with effective temperatures ranging from 5000 to 6500 K. The LTE wing profile of $\lambda 8542$ appears remarkably insensitive to the effective temperature in the interval $5000 < T_{\rm eff} < 6000\ K$.

This property is further illustrated in Fig. 10a which shows the depression in the line at $\lambda = 8539.0$ Å for dwarf models of different effective temperatures, with different metallicities. A similar diagram giving the depth at $\lambda = 8545.0$ Å shows exactly the same behaviour. However, in Fig. 10 as well as in Fig. 11, we see that this insensitivity to $T_{\rm eff}$ disappears progressively for non-solar metallicities or gravities.

5.3. Sensitivity to gravity

The variations of the predicted profiles of the $\lambda 8542$ line with gravity is shown in Fig. 12 for solar chemical composition models with effective temperatures of 6000, 5500 and 5000 K. At first sight the sensitivity to gravity appears quite large. For the two hotter models, the strong luminosity effect of the perturbation by the Paschen P15 line shows up quite conspicuously, in such a way that the behaviours of the blue wing and of the red wing turn out to be somewhat different. These properties are also well illustrated in Fig. 11 showing the variations of the line

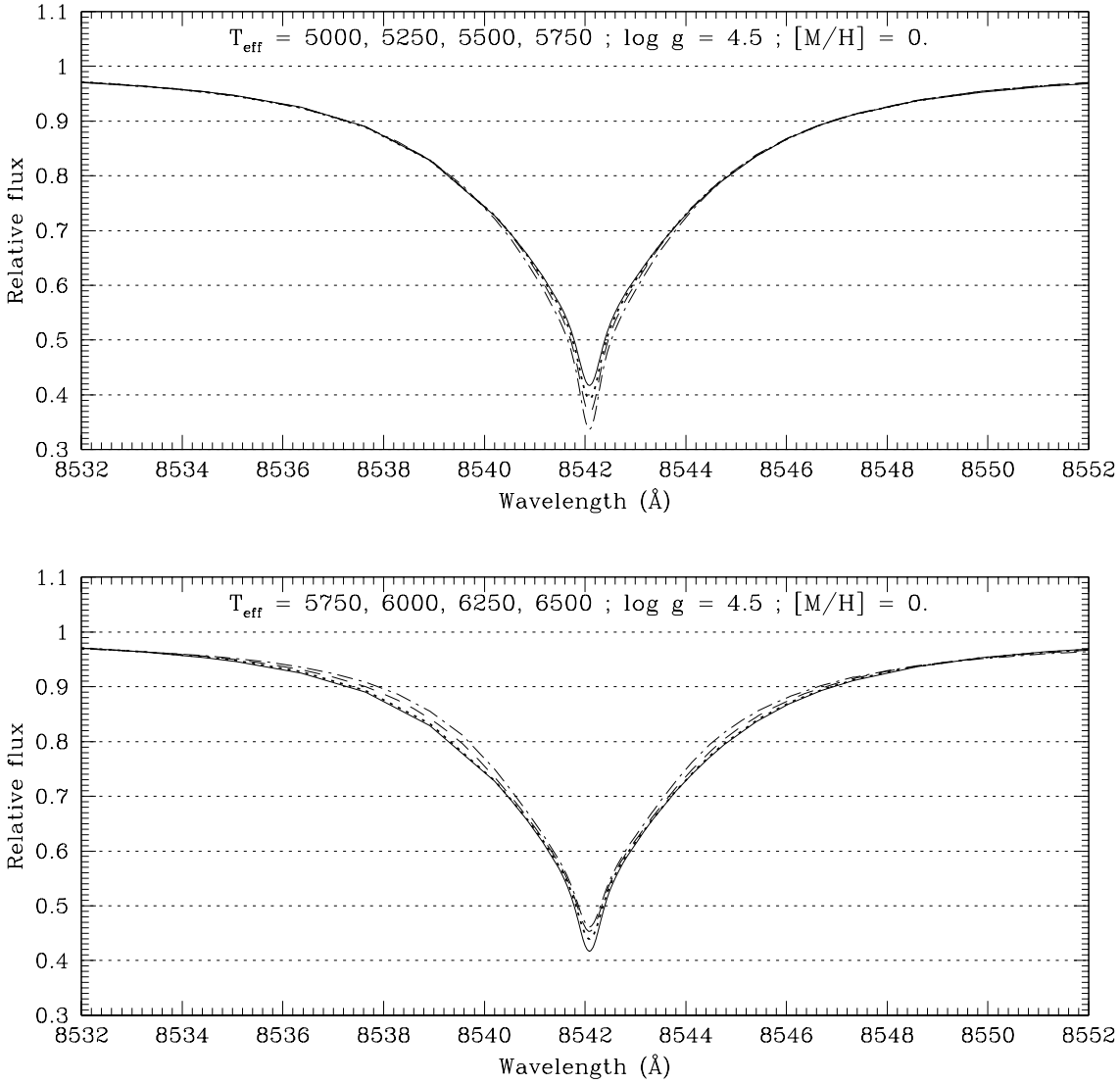

Fig. 9. Computed profiles of the Ca II $\lambda 8542$ line for dwarf stars with solar chemical composition and different effective temperatures. Upper panel: dot-dashed line $T_{\rm eff}$ = 5000; dashed, 5250; dotted, 5500; solid, 5750. Lower panel: solid $T_{\rm eff}$ = 5750; dotted, 6000; dashed, 6250; dot-dashed 6500.

depression at $\lambda = 8539$ Å (blue wing) and at $\lambda = 8545$ Å (red wing). The variation at $\lambda 8545$ is made more regular by the hydrogen line contribution. At $\lambda = 8539$, the effect of hydrogen is much less effective and we see the pure effect of gravity on the Ca II line: this effect is complicated and the observation of the line depression at this wavelength will not allow the sorting of stars by their different gravities. We further see that the sensitivity of the wings to gravity is only really significant for gravities $\log g \leq 3.0$. For dwarfs and subgiants the sensitivity to gravity is very weak and almost non-existent. For giants, assuming that the temperature and metallicity have already been determined independently, our computations show that the gravity could be derived from observed profiles of Ca II $\lambda 8542$ having a signal-to-noise ratio of 100 with an uncertainty between 0.10 and 0.15 in log g if $T_{\rm eff} \geq 5500\,K$. When $5000 < T_{\rm eff} < 5300$ K the uncertainty can reach ± 0.20 in log g. The Ca II IRT lines have often been advocated as a powerful luminosity indicator. These computations confirm that this statement needs to be qualified. The Ca II wings are only effective for cool giants and a reasonable accuracy can only be reached if the effects of temperature and metallicity are considered as well as those of gravity. An example of the use of the IRT lines for the determination of the gravity of Hyades giants is provided by Smith & Ruck (1997).

5.4. Sensitivity to metallicity

Fig. 13 shows the general behaviour of the Ca II $\lambda 8542$ line wing profile with changes in the global metallicity of dwarf stars model atmospheres. It is further illustrated in Fig. 10b which shows the variations of the line depression at $\lambda = 8539$ Å; an equivalent diagram for the depression at 8545 Å is completely similar. These variations are seen to be quite regular, contrary to the variations with gravity. The sensitivity to metallicity is

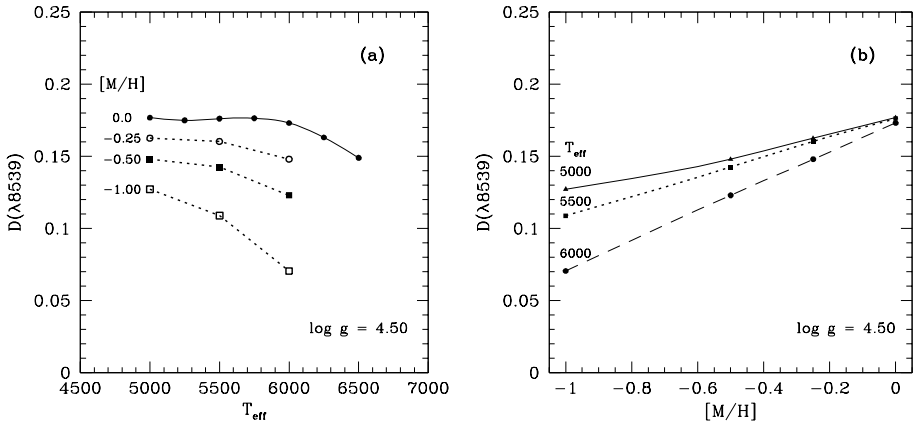

Fig. 10a and b. Sensitivity of the line depression at $\lambda 8539$ to **a** effective temperature and to **b** metallicity, as computed from dwarf stars model atmospheres.

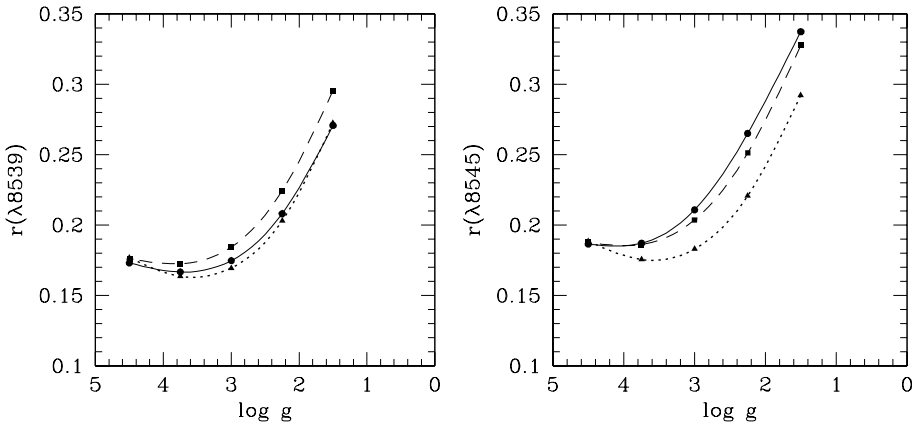

Fig. 11. Sensitivity of computed line depressions at $\lambda = 8539$ and at $\lambda = 8545$ Å to gravity. The solid line corresponds to models with $T_{\rm eff}$= 6000 K, the dashed line to $T_{\rm eff}$= 5500 K and the dotted line to $T_{\rm eff}$= 5000 K. All the models have a solar chemical composition.

higher for the hotter models. Therefore, the depression in the observed wings of $\lambda 8542$ may look like a good metallicity indicator provided that the stellar gravity has been determined beforehand with enough accuracy. Quantitatively, we can see that for a dwarf star (log g = 4.5) with $T_{\rm eff}$= 6000 K, the amplitude of the noise in an observation with a signal-to-noise ratio S/N = 100 is equivalent to the change in the depression at λ = 8539 or at λ = 8542 Å produced by a change in metallicity $|\Delta[M/H]| = 0.10$. At $T_{\rm eff}$= 5500 K the noise amplitude corresponds to $|\Delta[M/H]| = 0.15$ and at $T_{\rm eff}$= 5000 K to $|\Delta[M/H]| = 0.18$. We thus see that if we want to obtain a competitive accuracy on [M/H], say of ± 0.05, we have to use observations with S/N ratios higher than 200 for $T_{\rm eff}$= 6000 K and higher than 350 for $T_{\rm eff}$= 5000 K. The uncertainties induced by the errors on the model temperature and gravity are not taken into account by these figures. For Pop I dwarfs and subdwarfs the accuracy of the model parameters does not need to be very high, but for giants or metal-poor dwarfs the uncertainties on the temperature and gravity may be of much larger consequences.

6. Chromospheric activity

6.1. Chromospheric emission in the Ca II $\lambda 8542$ line

Linsky et al. (1979) demonstrated that the flux level in the central core of the Ca II $\lambda 8542$ line is a sensitive function of the level of stellar chromospheric activity as deduced from other observational sources, e.g. the core emission reversals in the H and K resonance lines of Ca II. Shine & Linsky (1972, 1974) had already discussed this sensitivity in the solar case in quiet regions compared to regions of various activity levels. In their observations of the Ca II $\lambda 8542$ line in a sample of 50 F8-K2 stars of all luminosity classes (at a resolution of 0.14 Å), Linsky et al. (1979) find no evidence for any central self-reversed emission feature (contrary to what is observed for bright plage regions in the Sun), but a clear filling-in of the central core in chromospherically active stars. They derive chromospheric radiative loss rates in this line which correlate well with rates in the Ca II H and K lines as well as with other activity indicators. However their non-LTE calculations of the Ca II $\lambda 8542$ line, for a simplified 3 levels plus continuum model Ca II ion and for different empirical model chromospheres, predict profiles which are not in good agreement with observed data. This happens even in the line wings which should be formed in conditions close to LTE and are consistently well represented by LTE synthetic profiles. According to J.J. Drake (1999, private communication) this unsatisfactory agreement may result from a poor choice of stellar parameters and to inappropriate model photosphere temperature structures.

Cayrel et al. (1983) estimated the level of activity in two solar type Hyades dwarfs, VB 64 and VB 73, from observations of the Ca II IRT lines. They carried out non-LTE calculations using three VAL model solar chromospheres (Vernazza et al. 1981) and a 5 levels plus continuum model Ca II ion. They obtain

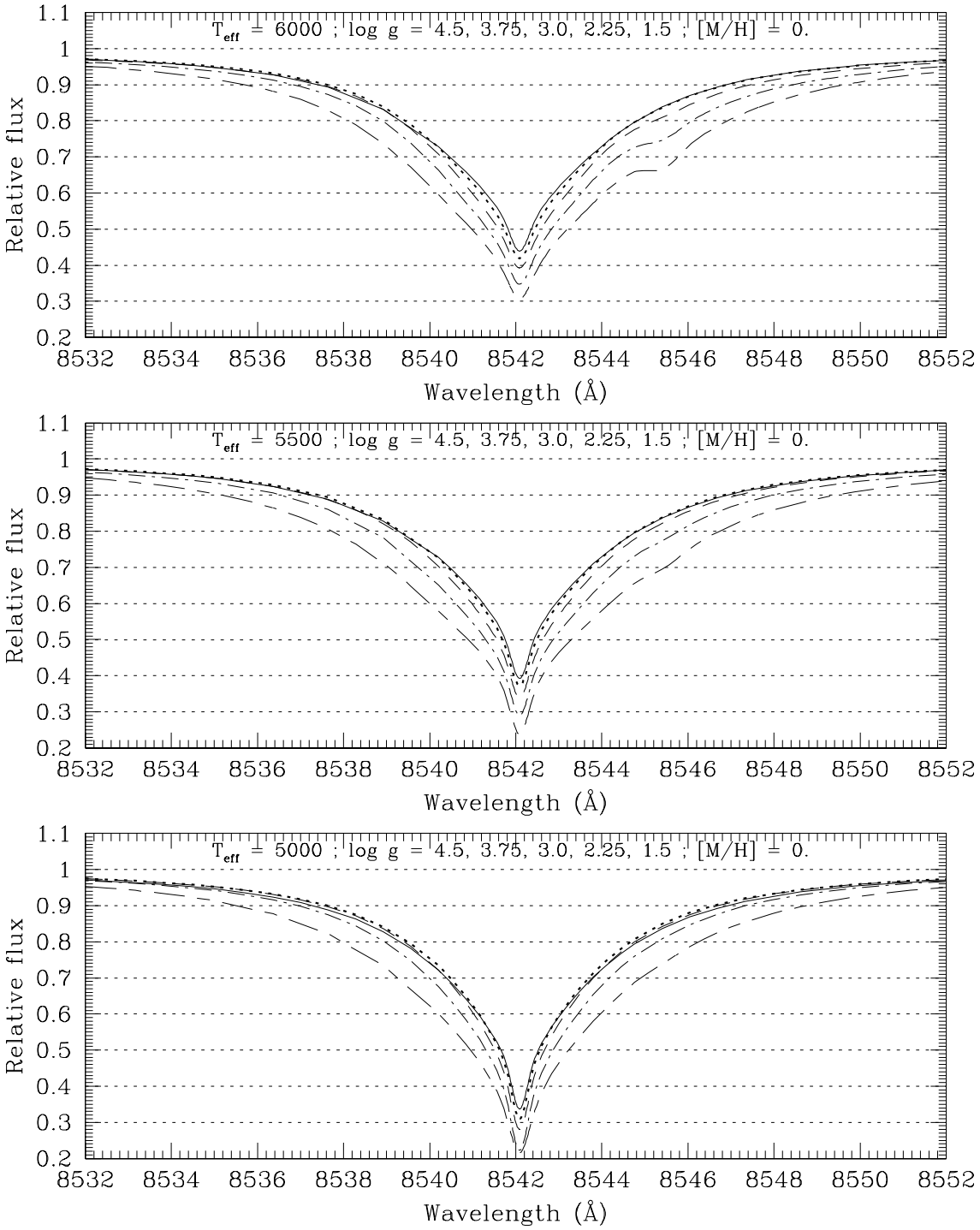

Fig. 12. Computed profiles of the Ca II $\lambda 8542$ line for solar composition stars with effective temperatures $T_{\rm eff}$= 6000, 5500 and 5000 K, for different values of gravity. Solid line for log g = 4.5, dotted for log g = 3.75, dashed for 3.0, dot-dashed for 2.25 and long dash - short dash for log g = 1.5.

line shapes in better qualitative agreement with the observations, which allow them to estimate the average activity of the Hyades dwarfs as equivalent to that of solar very bright network elements. Herbig (1985) used as a secondary activity indicator an index of chromospheric emission in the three IRT lines and showed this index to correlate very well with another index measuring the emission in the core of H_α. Similarly Soderblom et al. (1993b) used the emssion in the cores of H_α and Ca II $\lambda 8542$ to investigate the activity of the solar-type stars of the Pleiades.

The relation between the flux in the core of the Ca II IRT lines and stellar chromospheric activity has also been studied empirically by Foing et al. (1989) on higher resolution observa-

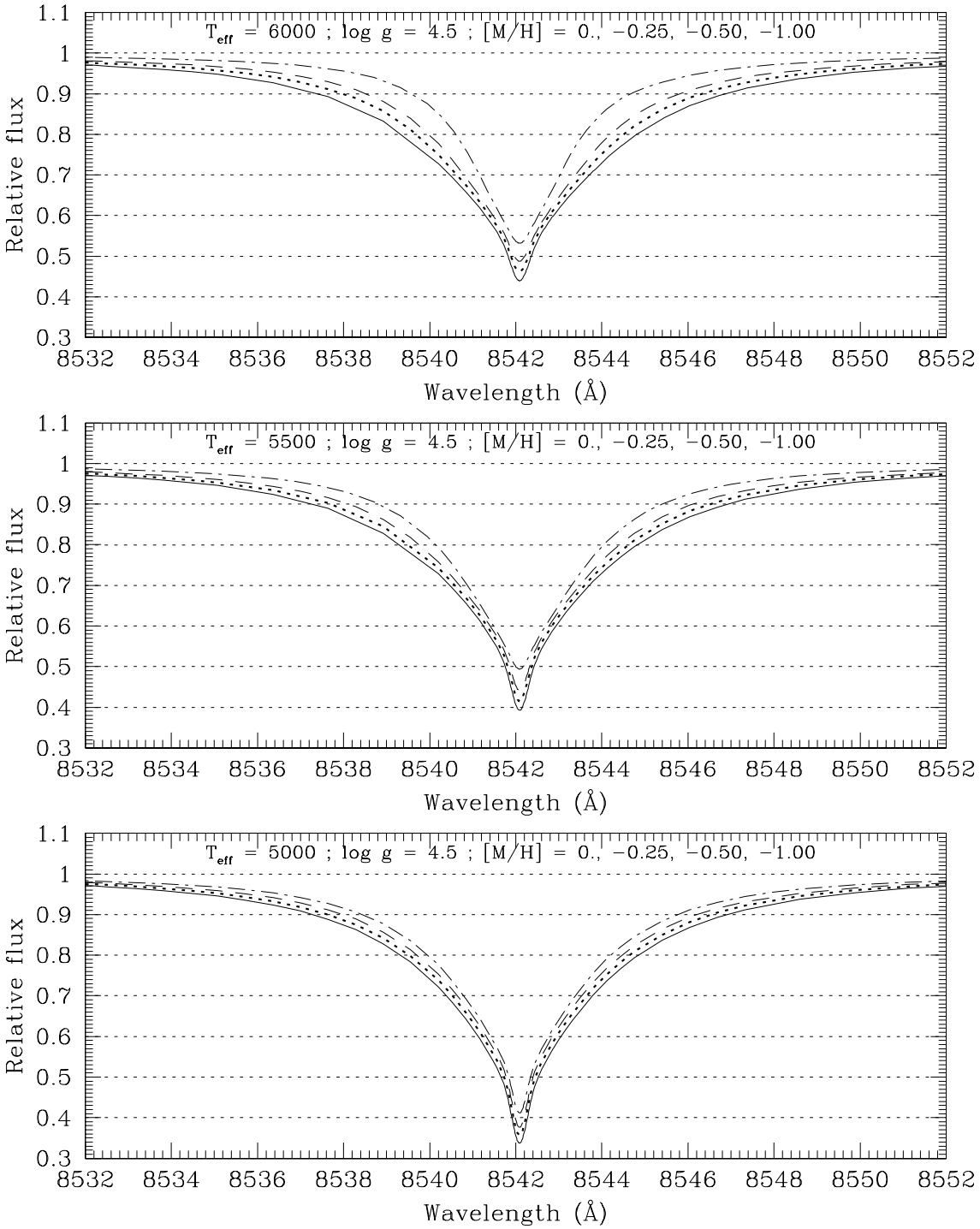

Fig. 13. Computed profiles of Ca II $\lambda 8542$ with dwarf models for the effective temperatures $T_{\rm eff}$= 6000, 5500 and 5000 K and different metallicities. Solid line for [M/H] = 0., dotted for -0.25, dashed for -0.50 and dot-dashed for [M/H] = -1.00.

tions of a sample of 16 F9-K4 dwarf and subgiant stars. Again the central depths of these lines are found to be very sensitive discriminators of stellar activity.

More data on the central depth of the $\lambda 8542$ line in dwarf or subgiant stars are scattered in the literature in tabular or graphical form, mostly in papers by the groups headed by G. Cayrel de Strobel or by G. Smith. Among the profiles published for active stars, a few do show central emission reversals like $\xi\ UMa\ B$ (Cayrel de Strobel et al. 1994) and HD 17925 (Cayrel de Strobel 1992); some others show conspicuous shoulders in their core, such as $\epsilon\ Eri$ (Drake & Smith 1993) or $\xi\ Boo\ A$ (Ruck & Smith 1995). This is contrary to the findings of Linsky et al. (1979), owing probably to the lower spectral resolution and photometric accuracy of their observations. Published central depths of

the $\lambda 8542$ line are collected in Table 4. Data for two specially well studied giants (Arcturus, $\alpha\ Boo$, and Pollux, $\beta\ Gem$) have been added to the table. The stars in Table 4 are all bright stars which have been submitted to detailed spectroscopic analysis. The "spectroscopic" effective temperatures of the stars, most often given in the references quoted in the table, are listed in column 2, and the normalized central depths of the $\lambda 8542$ line, D, are found in column 5. High chromospheric activity is often found in young stars; since high photospheric lithium abundance is also often associated with young stellar age, this abundance has been given in column 7 for comparison. Column 8 indicates whether the star is considered, on other grounds, as quiescent (a=0) or active (a=1).

Apart from the 0.14 Å resolution vidicon data of Linsky et al. (1979), all the other measurements of the central depths come from modern Reticon or CCD, high signal-to-noise (S/N) ratio spectra obtained with the Mc Donald 2.7 m, CFHT, ESO CAT-CES or OHP Aurélie coudé spectrographs in their higher resolution modes, which means that they are not very homogeneous. For some stars, several different measurements are available showing a significant dispersion, which can be noted already in the data of Linsky et al. (1979) or Foing et al. (1989). This dispersion may have a number of origins such as: scattered light in the spectrograph, resolution and S/N ratio effects, continuum location and stellar rotation rate. However, it is known that chromospheric emission varies with time in most of the stars, even the quietest. Repeated measurements on solar flux spectra show a typical dispersion of 0.015 which is similar to that of the other quiescent stars. The most active stars exhibit a much higher dispersion which cannot be explained in terms of instrumental effects only, and thus reflects real time variations in the level of activity of individual stars. Such variations, attributed to magnetic activity variations and stellar cycles, have been observed in the Ca II H and K central emission and have long been monitored and documented, especially at Mount Wilson (see references in next section). The value of the line depth given in Table 4 is an average of all measurements available; since there are only few measurements for each individual star, sometimes these averages may not be too well defined.

Fig. 14 shows the central depth as a function of effective temperature. There appears to be a clear dividing line between active and quiescent stars which shows some slope with effective temperature. A similar separation between active and quiescent stars was already observable in Fig. 4 of Foing et al. (1989).

6.2. Relation with the HK emission fraction

For many years, astronomers at Mount Wilson used the Ca II H and K lines as indicators of chromospheric emission. Vaughan & Preston, 1980 (VP) started an extensive survey of HK emission among northern late type dwarfs within 25 pc. They measured a chromospheric emission index, S, which is the ratio of the flux in the cores of the H and K lines to the flux in two 20 Å continuum windows on opposite sides of H and K. A definite time variability of the S index is found for almost all the stars. For many of them a clear rotational modulation is detected, leading to precise rotation periods. Noyes et al. (1984) studied the relationship between the rotation period and the HK emission strength. They characterized the emission strength by calculating, from the value of S, the ratio R_{HK} of the HK flux to the stellar bolometric flux, which is corrected for the photospheric contribution to the measured HK flux to yield R'_{HK}, a pure measure of the chromospheric emission. They could derive a tight empirical relation between the R'_{HK} emission strength and the Rossby number, i.e. the ratio of the rotation period to the convective turnover time. This relation was used by Soderblom (1985) to investigate the distribution of chromospheric emission and of angular velocities Ω of 177 nearby solar type dwarfs of the VP survey (northern hemisphere).

Henry et al. (1996) extended the VP survey to southern hemisphere solar type stars, providing R'_{HK} values for 746 targets. The histogram of the $\log\ R'_{HK}$ values (Figs. 5 and 8 of Henry et al.) shows a clear bimodal distribution, which had already been noted in the northern hemisphere survey by Vaughan & Preston (1980) and allows a rather clear separation between chromospherically active stars and low activity stars. A majority of low activity stars are distributed in a narrow peak around $\log\ R'_{HK} = -4.93$. A second group of stars, comprising about 30% of the sample, is distributed around a secondary mode at $\log\ R'_{HK} = -4.52$. Between the two modes, Henry et al. confirm the existence of the "Vaughan-Preston gap" (rather, a transition region), where very few stars are found with intermediate chromospheric emission fractions in the range $-4.75 < \log\ R'_{HK} < -4.60$. Henry et al. locate the dividing line between active and non-active stars at $\log\ R'_{HK} = -4.75$, although the minimum between the two modes is situated rather around a value of -4.67. The distribution of the chromospheric emission fractions must be interpreted bearing in mind the basic time variability of chromospheric emission. Typically, solar $\log\ R'_{HK}$ monthly means vary between -4.78 and -5.00. At the peak of its activity cycle the Sun may have $\log\ R'_{HK} = -4.75$ and its lowest activity during the Maunder Minimum corresponded to $\log\ R'_{HK} = -5.10$. Henry et al. (1996) argue that, in their time variation, stars very seldom slip from one mode into the other: the stars rather oscillate within the mode to which they belong. We might therefore consider that we are dealing with two groups showing distinct behaviours in their activity cycles. Henry et al. also identify a secondary transition zone at $\log\ R'_{HK} = -4.20$ separating *very* active stars (of which a significant fraction are close binary systems), as well as a distinct population of very quiescent solar type stars which, they suggest, may be currently in a Maunder Minimum type phase.

For most of the stars in our Table 4 measurements of the HK chromospheric emission fraction R'_{HK} are found in the papers of Henry et al. (1996), Soderblom (1985) or Noyes et al. (1984). For the three Hyades dwarfs R'_{HK} values are found in Duncan et al. (1984). For the visual double star $\xi\ UMa$ A+B, a value of R'_{HK} is found only for the integrated light of the two components A+B. As B is the very active component whereas A shows a rather low activity (Cayrel de Strobel et al. 1994), the

Table 4. Observed central depressions of the Ca II $\lambda 8542$ line found in the literature, in relation to the Mount Wilson R'_{HK} activity index.

HD	$T_{\rm eff}$	$\log g$	[M/H]	CD	$\log R'_{HK}$	N(Li)	a	Ref	Name
$\log g > 4.0$									
0	5777	4.44	0.00	0.75	-4.89	1.1	0		Sun
1835	5780	4.50	+0.17	0.57	-4.44	2.5	1	12	$9\,Cet$
4614	5890	4.40	-0.24	0.69	-4.96		0	19	$\eta\,Cas\,A$
10700	5380	4.50	-0.53	0.74	-4.96	< 0.5	0	12,14,19	$\tau\,Cet$
17925	5090	4.60	+0.10	0.46	-4.30	2.5	1	2	
20630	5630	4.50	+0.04	0.60	-4.45	2.0	1	4,12,14	$\kappa^1 Cet$
22049	5180	4.75	-0.09	0.58	-4.47	< 0.5	1	11,12,14	$\epsilon\,Eri$
26965	5090	4.31	-0.34	0.77	-4.91		0	12,14	$o^2 Eri$
27959	5840	4.44	+0.03	0.59	-4.43	2.5	1	20	VB 52
28099	5770	4.50	+0.14	0.60	-4.47	2.3	1	15,20,21	VB 64
28344	5900	4.50	+0.14	0.59	-4.42	2.7	1	20,21	VB 73
35296	6150	4.36	0.00	0.53	-4.40		1	14	$111\,Tau$
38392	4950	4.50	+0.02	0.58	-4.50	< -0.2	1	3	$\gamma\,Lep\,B$
39587	5900	4.50	-0.05	0.58	-4.46		1	14	$\chi^1 Ori$
44594	5780	4.50	+0.15	0.75	-4.92	1.2	0	4	
53705	5870	4.30	-0.25	0.75	-4.93	1.1	0	8	
53706	5290	4.50	-0.28	0.77	-5.01	< 0.4	0	8	
76151	5710	4.50	+0.06	0.70	-4.68	1.7	0	4	
98230	5650	4.50	-0.34	0.38	-4.34	< 0.8	1	1	$\xi\,UMa\,B$
98231	5950	4.30	-0.36	0.69		2.3	0	1	$\xi\,UMa\,A$
100623	5230	4.60	-0.38	0.75	-4.86	< 0.8	0	9	
102870	6090	4.20	+0.10	0.80	-5.03	2.0	0	4	$\beta\,Vir$
103095	5170	4.50	-1.30	0.72	-4.90	< 0.5	0	17	Gmb 1830
114710	5960	4.40	-0.02	0.73	-4.73	2.4	0	17	$\beta\,Com$
115617	5585	4.50	-0.02	0.76	-4.98	< 0.8	0	14,15	$61\,Vir$
125072	4965	4.50	+0.26	0.67		< 0.8	1	15	
128620	5800	4.31	+0.22	0.80	-5.00	1.3	0	7,12	$\alpha\,Cen\,A$
128621	5325	4.58	+0.26	0.79	-4.92	< 0.4	0	7,12	$\alpha\,Cen\,B$
131156	5500	4.60	-0.15	0.47	-4.34		1	12,14,16	$\xi\,Boo\,A$
131977	4625	4.79	+0.01	0.72	-4.48		1	12	
147513	5830	4.30	-0.10	0.61	-4.52		1	12	
147584	6030	4.50	-0.19	0.62	-4.56	2.9	1	12	$\zeta\,Tr\,A$
155885	5100	4.60	-0.30	0.65	-4.57	< -0.2	1	3	$36\,Oph\,B$
155886	5125	4.60	-0.29	0.61	-4.57	< -0.2	1	3	$36\,Oph\,A$
156026	4550	4.70	-0.36	0.61	-4.49	< 0.5	1	3	$36\,Oph\,C$
156274	5295	4.50	-0.35	0.76	-4.94	< 0.8	0	15	$41\,Ara$
165341	5345	4.50	-0.05	0.60	-4.59		1	12,14	$70\,Oph\,A$
186408	5785	4.28	+0.06	0.76		1.2	0	13	$16\,Cyg\,A$
186427	5760	4.35	+0.02	0.76		< 0.4	0	13	$16\,Cyg\,B$
190422	6180	4.50	-0.13	0.53	-4.38	2.9	1	5	
209100	4545	4.60	-0.10	0.73	-4.56	< -0.3	1	12	$\epsilon\,Ind$
$\log g < 4.0$									
2151	5830	3.84	-0.20	0.78	-5.00	2.4	0	12	$\beta\,Hyi$
62509	4865	2.75	-0.04	0.84		0.6	0	10	$\beta\,Gem$
81809	5630	3.75	-0.31	0.73	-4.98	1.1	0	4	
124897	4375	1.60	-0.60	0.87		< -0.8	0	18	$\alpha\,Boo$
150680	5825	3.78	+0.05	0.78		< 0.8	0	6	$\zeta\,Her\,A$
188512	5225	3.79	-0.13	0.86	-5.15		0	14	$\beta\,Aql$
190248	5540	3.80	+0.28	0.82	-5.00	< 0.7	0	12	$\delta\,Pav$

References: (1) Cayrel de Strobel et al. 1994; (2) Cayrel de Strobel 1992; (3) Cayrel de Strobel et al. 1989; (4) Cayrel de Strobel & Bentolila 1989; (5) Chmielewski 1999 (in preparation); (6) Chmielewski et al. 1995; (7) Chmielewski et al. 1992; (8) Chmielewski et al. 1991; (9) Cristaldi 1992; (10) Drake & Smith 1991; (11) Drake & Smith 1993; (12) Foing et al. 1989; (13) Friel et al. 1993; (14) Linsky et al. 1979; (15) Perrin et al. 1988; (16) Ruck & Smith 1995; (17) Smith et al. 1992; (18) Smith & Drake 1990; (19) Smith & Drake 1987; (20) Smith & Ruck 1997; (21) Cayrel et al. 1983.

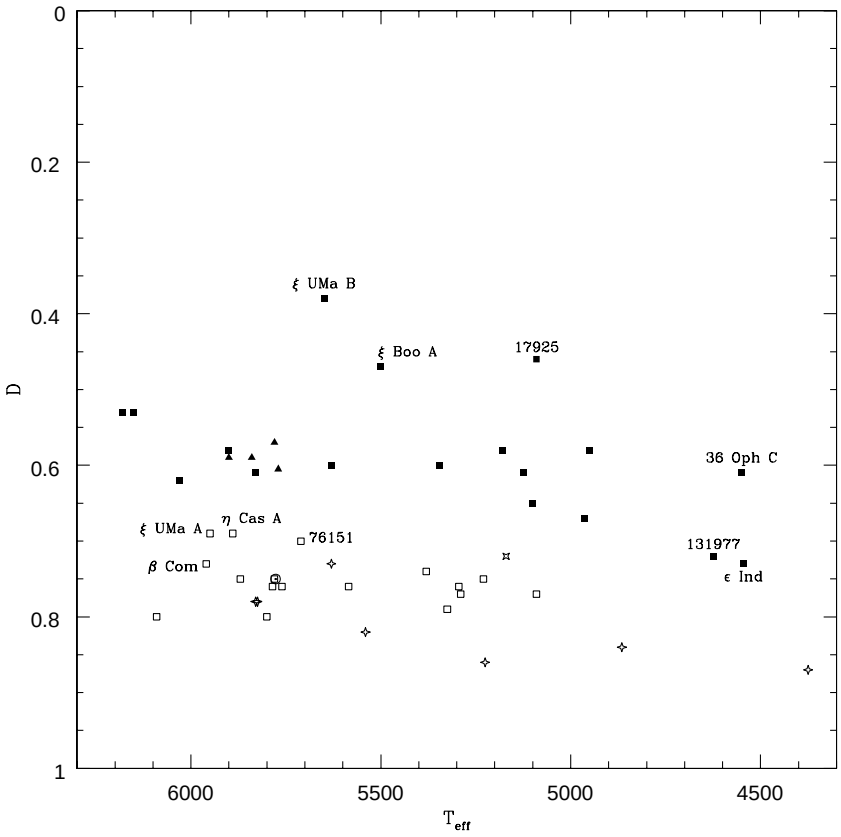

Fig. 14. Mean observed depressions at the center of the $\lambda 8542$ line as a function of effective temperature. Filled squares represent active dwarf stars and open squares stand for quiescent dwarfs. The three Hyades dwarfs, VB 52, VB 64, VB 73, and 9 Cet (HD 1835, a member of the Hyades moving group) are represented by filled triangles. The Sun is represented by an open circle and the subdwarf Gmb 1830 by a cross. The "plus" signs correspond to evolved stars which, in this sample, are all reputed to be quiescent.

R'_{HK} value has been attributed to component B in Table 4. The average values of $\log\ R'_{HK}$ are given in column 6 of the table. Fig. 15 shows the Ca II $\lambda 8542$ line central depth, D, versus $\log\ R'_{HK}$, with vertical and horizontal bars joining extreme values of D, as well as of $\log\ R'_{HK}$, found in the literature for each star (they should not be interpreted as error bars). To be really meaningful the average values and the variability bars should result from long time monitoring of the stars, which is not the case for most D and many R'_{HK} values. Despite this drawback, we find a good correlation between the average values of D and $\log R'_{HK}$.

A few interesting stars are identified in Fig. 15. This figure illustrates, on our limited sample with unclear selection effects, the conclusions drawn by Henry et al. (1996), namely that the stars group into two distinct modes, with only very few stars showing an intermediate level of activity.

Considering the variability and inhomogeneity of the data, a mathematical description of the relation between D and $\log R'_{HK}$ should be as simple as possible. Clearly a linear relation is not adequate and some curvature is required. A simple parabolic fit gives a good overall representation of the data but shows a minimum at $\log R'_{HK} = -4.96$ which is not physically meaningful (this is near the maximum of the distribution of the low activity stars). As the level of chromospheric activity decreases, the central depth of the $\lambda 8542$ line should saturate to a value not reaching 100%, which may depend on the stellar atmospheric parameters; the distribution of $\log R'_{HK}$ for low activity stars reaches zero at $\log R'_{HK} = -5.10$ and there are only very few stars with $\log R'_{HK} < -5.10$. This is why the relation between D and $\log R'_{HK}$ is expected to be rather flat at this limit. It seemed therefore reasonable to represent this relation by a parabola constrained to have its minimum at $(\log R'_{HK})_{min} = x_m = -5.10$. If $x = \log R'_{HK}$ and $y = D$, such a parabola is described by the formula:

$$y = ax^2 - 2ax_m x + c$$

A least-squares fit to the data, eliminating stars discrepant by more than 3σ, yields a = -0.496 and c = -12.12, with a scatter σ = 0.022, and the resulting curve is drawn in Fig. 15. Attempts to fit the data by a branch of hyperbola appeared less convincing. Inspection of Fig. 15 confirms that D is a good discriminator between low and high activity stars. Fig. 14 suggests that, in the variable D, the location of the boundary between low and high activity stars changes with the stellar effective temperature and the dividing line thus seems to have a significant slope in the diagram. In Fig. 15 the symbols representing the stars are coded according to their effective temperature (see insert). Unfortunately, given the limited size of the sample and limited accuracy of the data, we cannot see any obvious temperature effect on the mean relation between the two variables.

6.3. Discussion

The star $\beta\ Aql$ belongs to the rare population of extremely low activity stars suggested by Henry et al. to be in a Maunder Minimum type phase: the $\lambda 8542$ line in this star is also the deepest ever reported in the literature (except for the cool giant Arc-

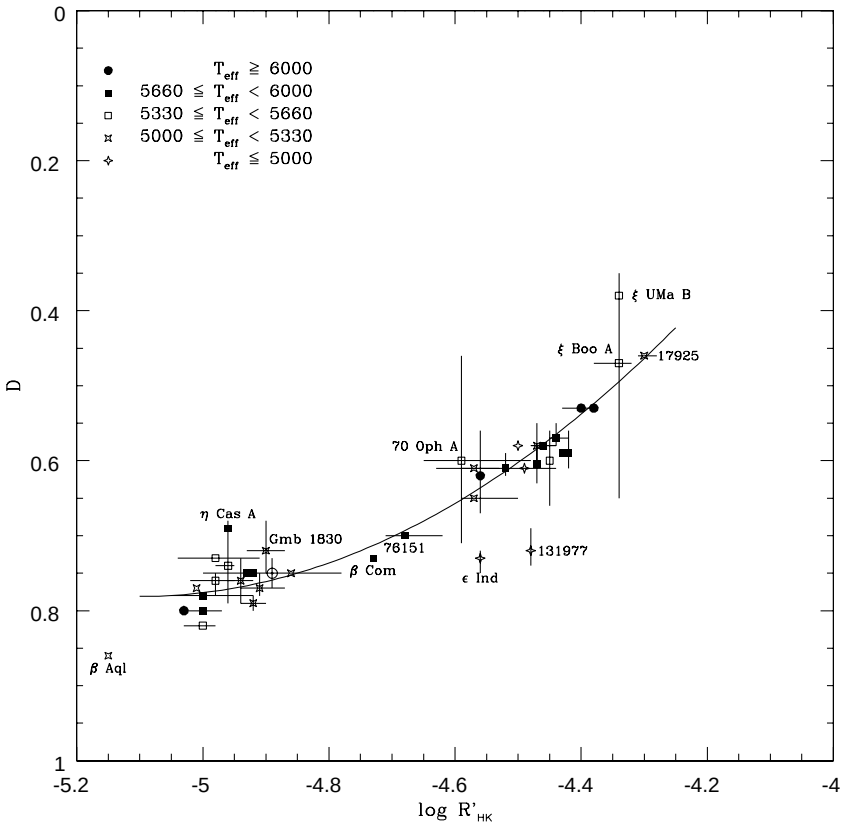

Fig. 15. Central depression of the $\lambda 8542$ line versus the HK emission fraction index. The horizontal and vertical bars connect the extreme values recorded for each parameter when several measurements can be found in the literature. An average relation between the activity indices is shown by the continuous curve. A few interesting stars are identified.

turus). A fit by a parabola constrained to have a minimum at $x_m = -5.15$, instead of -5.10, does not produce a significantly different representation.

The location and variability of the high velocity subdwarf Gmb 1830 in Figures 14 and 15 is not among the least active stars, which might suggest that this very old, slowly rotating Population II star has kept some degree of chromospheric activity. This, however, raises the question of the sensitivity of our activity indicators to the stellar parameters (Drake 1999). Clearly, changes in gravity or abundance will affect the opacity and depth of formation of the lines. Figs. 12 and 13 show that, if the line core of $\lambda 8542$ were formed in LTE, the central depth of the line would be shallower for decreasing metallicities and deeper for lower gravities. The line might be shallower in Gmb 1830 just on account of the lower calcium abundance. A realistic treatment of the problem would require non-LTE computations that go beyond the scope of this paper.

Two stars on the diagram, $\epsilon\ Ind$ and HD 131977, stand out as discrepant with the overall representation, lying at more than 4.5σ under the mean relation: they belong to the high activity group according to their $\log R'_{HK}$ whereas the depth of their $\lambda 8542$ line is comparable with that of lower activity stars. This discrepancy may have to do with the fact that, as seen in Fig. 14, they are at the low effective temperature end of our sample; on the other hand, $36\,Oph\,C$, which has a similar temperature, is not discrepant in Fig. 15. Yet, Erdelyi-Mendes and Barbuy (1991) have shown the growing pollution of the Ca II IRT spectral region by lines of the molecules CN and TiO at temperatures lower than about 4500 K; it may seriously affect the localization of the continuum (see, in particular, their Fig. 1c). Unfortunately, raising the continuum would go in the "wrong" direction, making the $\lambda 8542$ line still deeper!

The above representation describes only first order effects. The treatment of the effective temperature effects would require more homogeneous data with averages based on long time baselines, and would represent a heavy observational load. The chromospheric HK emission fraction, R'_{HK}, is derived by subtracting an estimated photospheric contribution from the total emission fraction R_{HK}. This correction is carried out on the basis of the $(B-V)$ colour index, assuming a unique relation between $(B-V)$ and $T_{\rm eff}$. This photospheric correction could thus be somewhat improved. For a direct comparison between $\log R'_{HK}$ and the depth D of the Ca II $\lambda 8542$ line, this last parameter ought to be transformed into another chromospheric emission fraction, also corrected for the effects of the basic atmospheric parameters. Such a transformation is not easy to devise. A purely theoretical approach is beyond reach at the present time. It would require realistic non-LTE computations based on adequate model photospheres (remember also the upper depth-scale truncation problem mentioned above in Sect. 4). An empirical approach is also difficult since it is established that there are no really steady, chromospherically inactive stars. Practically, the Maunder-Minimum stars in the sample of Henry et al. could be used as references if they turned out to provide a dense enough network. Most of the stars in this group are subgiants of luminosity class IV. The $(B-V)$ colours of all

the very quiescent stars ($\log R'_{HK} < -5.15$) in the sample of Henry et al. fall in the range $0.54 < (B-V) < 0.92$, roughly corresponding to temperatures $5200 < T_{\rm eff} < 6300\,K$. There is thus unfortunately no star in this sample which could be used as a convenient zero-activity standard in the lower temperature range, $T_{\rm eff} < 5000\,K$. Note that R'_{HK} is not defined either for $(B-V) > 1.0$.

Other stars stand abnormally high above the mean curve in Fig. 15. The star $\eta\ Cas\ A$ lies at 3.6σ above the mean relation. Its lines are significantly rotationally broadened ($v \sin i \approx 6\ km\ s^{-1}$). It has been observed only once in each of the coordinates. More observations are required before definite conclusions can be drawn from its location on the diagram. Another star, $\xi\ UMa\ B$, is found high (5.6σ) above the mean curve. It belongs to the exotic visual binary system $\xi\ UMa\ A+B$ (actually a quadruple system) discussed in detail by Cayrel de Strobel et al., 1994 (see also Pallavicini et al. 1987).

As a general scheme, high chromospheric activity, high rotation velocity and high surface lithium abundance are associated with young stellar age. At constant age, in main sequence stars cooler than $T_{\rm eff} \approx 6200\,K$, the surface lithium abundance decreases dramatically with decreasing effective temperature (or decreasing mass). There are, however, notorious exceptions to these general rules. The old evolved star $\beta\ Hyi$ (solar mass, but twice the solar age) is one of them: it has low activity, slow rotation, but a very high photospheric lithium content. Pasquini et al. (1994) show that the case of βHyi is not truly exceptional: they confirm the existence of an important group of field G dwarfs with high Li content but apparently old age and conclude that a high Li abundance is a necessary but not sufficient condition for a star to be young. In young open clusters Soderblom et al. (1993a,1993b) and Soderblom (1995) show that, at a given color, there is a large scatter in activity and rotation as well as in the Li content, with the most rapidly rotating stars having the most Li. Yet, in the somewhat older Hyades cluster, a tight relation between Li content and stellar mass is established. The complicated picture that emerges may find an explanation in theories by Pinsonneault et al. (1989,1990) based on the transport of angular momentum from the stellar core outwards, implying that the abundance of Li depends more on the rotational history of the star rather than on rotation *per se*. The above mentioned $\xi\,UMa\,A+B$ system also appears to be contradictory with the general picture. Each of the two components is itself a spectroscopic binary, and the system is better described as Aa + Bb. The study of Cayrel de Strobel et al. (1994) establishes that the spectrum of Aa shows a rather weak chromospheric activity and strong lithium abundance, whilst the spectrum of Bb indicates a temperature cooler than Aa by about 300 K (from H_α), a high chromospheric activity (from H_α as well as from the Ca II IRT) and undetectable lithium. The age of the system is bound between 2 and 8 Gyr, and the masses of the main components A and B are very similar, being $\approx 0.85 \mathcal{M}_\odot$. The Bb system has quite a small orbital period of 3.98d, which suggests that the rotation period of this tight system is tidally locked to the orbital period. Cayrel de Strobel et al. explain that the high activity of $\xi\,UMa\,B$ is due to its high rotation rate, and the abnormally low surface lithium abundance owes to the unusual mass loss rate caused by high activity maintained during several Gyr. A similar situation is found in RS Cvn binaries (Randich & Palavicini, 1991). This is all consistent with the now widely accepted idea that the real basic link is between high activity and high rotation rate. The question of the surface lithium content is somewhat more complicated.

Two of the stars listed in Table 4 fall into the Vaughan-Preston gap of intermediate activity stars according to their HK emission fraction. As seen in Fig. 14, the depth of the $\lambda 8542$ line of HD 76151 falls on the upper edge of the area populated by low activity stars. The case of $\beta\ Com$ is less clear. Here again more measurements are needed before reaching conclusions. It is interesting to note that the two stars have a high lithium abundance. I could not find any individual measurement of R'_{HK} for $\xi\ UMa\ A$ (the separation between $\xi\ UMa\ A$ and B is only 2.5 arc sec). Given its high surface lithium content and its location in Fig. 14, we expect $\xi\ UMa\ A$ to be in the group of intermediate activity stars. Should this make us favour the lower bound of the age bracket of the system? It would in any case be interesting to monitor the activity in this visual double system in order to find the extent of variability of the two components and find eventual rotational modulations allowing to find the true rotation periods (the lines in their spectra are not obviously rotationally broadened and the system is probably seen pole-on).

7. Conclusions

The purpose of the computations presented in this paper was to sum up the diagnostic capabilities provided by observations of the profiles of the infrared triplet lines of ionized calcium. It has first been stressed that the local continuum level in the region of the Ca II IRT in the solar spectrum cannot be correctly described without taking into account the cumulative absorption by the hydrogen Paschen lines. As a consequence, the determination of the continuum of stellar observations in this region has to be carried out with special caution. It was then shown that the observed solar flux profiles of the LTE wings of the Ca II IRT can be well represented by computations based on two of the most popular empirical model solar photospheres (MACKKL and Holweger). Calculations based on theoretical solar photospheres proved significantly less successful. This confirms and illustrates what was already found and exploited by Smith, Drake and collaborators, i.e. that the wing profiles of the Ca II IRT provide a good test for the adequacy of a model temperature distribution for a given star. The values of the hydrogen damping constant of these lines leading to the best fits of the solar flux observations are consistent with the values determined by Smith & Drake (1988) from high quality solar intensity observations. It also turned out that the computed profiles are not very sensitive to the exact temperature variation law of the hydrogen damping constant which can very well be represented in the commonly used van der Waals approximation.

The differential sensitivity of the line profiles to the basic stellar atmospheric parameters was investigated through computations of the $\lambda 8542$ line with photospheres from the ho-

mogeneous GBEN grid of theoretical model atmospheres. The contribution of the Paschen lines cannot be ignored for dwarfs of effective temperature higher than 5800 K; for giant stars, it has to be taken into account down to 5500 K, or even cooler for the brightest ones. Otherwise, these computations generally confirm conclusions already reached by Smith & Drake (1987, 1990) and extended to cooler stars by Erdelyi-Mendes & Barbuy (1991). The wing profiles are remarkably insensitive to temperature for solar type dwarf stars with $5000 < T_{\rm eff} < 6000\,K$; this property breaks off however for more luminous or metal-poor stars. Their behaviour with variations of the stellar gravity is not as simple as sometimes advocated: the sensitivity of the wing profiles to gravity is only effective for $\log g < 3.0$. By contrast, the variations with changes in the metallicity are much smoother and the depression in the wings of this line may be used as an indicator of the calcium abundance provided that the temperature and gravity of the star have been previously determined with reasonable accuracy and that the available observed spectra have a rather high signal-to-noise ratio. Relations such as those proposed by Diaz et al. (1989) or Zhou (1991) keep a statistical interest for studies of homogeneous stellar populations. However, for the determination of stellar parameters of individual stars, it is usually not difficult to find more sensitive spectroscopic indicators, especially for dwarf and subgiant stars.

The central depth of the chromospheric core or the $\lambda 8542$ line is a good indicator of the level of chromospheric activity of a star. A simple average relation has been found between it and the Mount-Wilson activity indicator $\log R'_{HK}$. However, owing to the intrinsic variability of chromospheric activity, systematic studies of this phenomenon must ensure sufficient time sampling to cover such phenomena as rotational modulation (periods of the order of a month) or activity cycles (periods of the order of 10 years), which require great instrumental stability and reproductibility. In that respect, specialized spectrophotometers, such as the Mount-Wilson instrument, are best suited and much more efficient.

Acknowledgements. I am particularly indebted to Dr Giusa Cayrel de Strobel who shared some of her very nice observations with me. I also thank Dr K. Eriksson for providing me with the GBEN grid of model atmospheres and Gerlind Brandès for kindly correcting the awkwardness of my English. This paper owes much to the corrections, constructive comments and suggestions by the referee, Dr J.J. Drake.

References

Baschek B., Holweger H., Traving G., 1966, Abhandl. Hamburger Sternw. **VIII**, 26
Bell R.A., Eriksson K., Gustafsson B., Nordlund A., 1976, A&AS 23, 37
Carquillat J.M., Jaschek C., Jaschek M., Ginestet N., 1997, A&AS 123, 5
Cayrel R., Cayrel de Strobel G., Campbell B., Mein N., Mein P., Dumont S., 1983, A&A 123, 89
Cayrel de Strobel G. 1992, The Messenger (ESO) 70, 37
Cayrel de Strobel G., Bentolila C., 1989, A&A 211, 324
Cayrel de Strobel G., Cayrel R., Friel E., Zahn J.-P., Bentolila C., 1994, A&A 291, 505
Cayrel de Strobel G., Perrin M.-N., Cayrel R., Lebreton Y., 1989, A&A 225, 369
Chapelle J., Sahal-Bréchot S., 1970, A&A 6, 415
Chmielewski Y., Cayrel de Strobel G., Cayrel R., Lebreton Y., Spite M., 1995, A&A 299, 809
Chmielewski Y., Cayrel de Strobel G., Lebreton Y., Bentolila C., 1991, A&A 247, 368
Chmielewski Y., Friel E., Cayrel de Strobel G., Bentolila C., 1992, A&A 263, 219
Cristaldi S. 1992, Travail de diplôme, Observatoire de Genève
Diaz A.I., Terlevich E., Terlevich R., 1989, MNRAS 239, 325
Drake J.J., 1999, private communication
Drake J.J., 1991, MNRAS 251, 369
Drake J.J., Smith G., 1991, MNRAS 250, 89
Drake J.J., Smith G., 1993, ApJ 412, 797
Duncan D.K., Baliunas S.L., Noyes R.W., Vaughan A.H., Frazer J., Lanning H.M., 1984, PASP 96, 707
Edvardsson B., Andersen J., Gustafsson B., Lambert D.L., Nissen P.E., Tomkin J., 1993, A&A 275, 101
Erdelyi-Mendes M., Barbuy B., 1991, A&A 241, 176
Eriksson K., Bell R.A., Gustafsson B., Nordlund A., 1979, Trans. IAU, Vol. 17A, Part 2, Reidel, Dordrecht, p. 200
Foing B.H., Crivellari L., Vladilo G., Rebolo R., Beckman J.E., 1989, A&AS 80, 189
Friel E., Cayrel de Strobel G., Chmielewski Y., Spite M., Lebre A., Bentolila C., 1993, A&A 274, 825
Gallagher A., 1967, Phys. Rev. 157, 24
Ginestet N., Carquillat J.M., Jaschek M., Jaschek C., 1994, A&AS 108, 359
Gustafsson B., Bell R.A., Eriksson K., Nordlund A., 1975, A&A 42, 407
Henry T.J., Soderblom D.R., Donahue R.A., Baliunas S.L., 1996, AJ 111, 439
Herbig G.H. 1985, AJ 289, 269
Holweger H., 1972, Solar Phys. 25, 14
Holweger H., Müller E.A., 1974, Solar Phys. 39, 19
Jones J.E., Alloin D.M., Jones B.J.T., 1984, ApJ 283, 457
Jørgensen U.G., Carlsson M., Johnson H.R., 1992, A&A 254, 258
Kurucz R.L., 1992, Rev. Mexicana Astron, Astrof. 23, 181
Kurucz R.L., Furenlid I., Brault J., Testerman L., 1984, "Solar Flux Atlas from 296 to 1300 nm", National Solar Observatory, Sunspot (N.M.)
Linsky J.L., Hunten D.M., Sowell R., Glackin D.L., Kelch W.L., 1979, ApJS 41, 481
Mallik S.V., 1997, A&AS 124, 359
Maltby P., Avrett E.H., Carlsson M., Kjeldseth-Moe O., Kurucz R.L., Loeser R., 1986, ApJ 306, 284
Noyes R.W., Hartmann L.W., Baliunas S.L., Duncan D.K., Vaughan A.H., 1984, ApJ 279, 763
O'Neill J.A., Smith G., 1980, A&A 81, 100
Pallavicini R., Cerruti-Sola M., Duncan D.K., 1987, A&A 174, 116
Pasquini L., Liu Q., Pallavicini R., 1994, A&A 287, 191
Perrin M.-N., Cayrel de Strobel G., Dennefeld M., 1988, A&A 191, 237
Pinsonneault M.H., Kawaler S.D., Demarque P., 1990, ApJS 73, 21
Pinsonneault M.H., Kawaler S.D., Sofia S., Demarque P., 1989, ApJ 338, 424
Praderie F., 1967, Ann. Astrophys. 30, 31
Randich S., Pallavicini R., 1991, Mem. Soc. Astron. Ital. 62, 75

Ruck M.J., Smith G., 1995, A&A 304, 449
Shine R.A., Linsky J.L., 1972, Solar Phys. 25, 357
Shine R.A., Linsky J.L., 1974, Solar Phys. 39, 49
Smith G., 1981, A&A 103, 351
Smith G., 1988, J. Phys. B 21, 2827
Smith G., Drake J.J., 1987, A&A 181, 103
Smith G., Drake J.J., 1988, MNRAS 231, 115
Smith G., Drake J.J., 1990, A&A 231, 125
Smith G., Lambert D.L., Ruck M.J., 1992, A&A 263, 249
Smith G., O'Neill J.A., 1975, A&A 38, 1
Smith G., Raggett D.St.J., 1981, J. Phys. B 14, 4015
Smith G., Ruck, M.J., 1997, A&A 324, 1091
Soderblom D.R., 1985, AJ 90, 2103
Soderblom D.R., 1995, Mem. Soc. Astron. Ital. 66, 347
Soderblom D.R., Jones B.F., Balachandran S., Stauffer J.R., Duncan D.K., Fedele S.B., Hudon J.D., 1993a, AJ 106, 1059
Soderblom D.R., Stauffer J.R., Hudon J.D., Jones B.F., 1993b, ApJS 85, 315
Vaughan A.H., Preston G.W., 1980, PASP 92, 385
Vernazza J.E., Avrett E.H., Loeser R., 1981, ApJS 45, 635
Watanabe T., Steenbock, W., 1985, A&A 149, 21
Zhou X., 1991, A&A 248, 367